Images of Adsorbates with the Scanning Tunneling Microscope: Theoretical Approaches to the Contrast Mechanism

Philippe Sautet

Institut de Recherches sur la Catalyse, CNRS, 2 Av. A. Einstein, 69626 Villeurbanne Cedex, France, and Laboratoire de Chimie Théorique, Ecole Normale Supérieure de Lyon, 46 Allée d'Italie, 69364 Lyon Cedex 07, France

Received November 20, 1996 (Revised Manuscript Received March 6, 1997)

Contents

Philippe Sautet is born in Provence, France, in 1961. He graduated from the "Ecole Polytechnique", Palaiseau, and in 1989 he defended a Ph.D. thesis in Theoretical Chemistry at the Paris XI University (Orsay). He obtained at that date a permanent research position at "Centre National de la Recherche Scientifique" (CNRS). His research interest is the quantum chemical study of the interaction between a molecular adsorbate and a solid surface, in relation with elementary steps of catalysis. One important topic is the calculation and interpretation of the images of surfaces obtained with the scanning tunneling microscope, for which he developed a dedicated code. In order to achieve a detailed comparison with experimental data and to build qualitative elements for a better understanding of the STM image contrast mechanism, he spent one year in 1991–1992 in the group of Miquel Salmeron at the Lawrence Berkeley Laboratory. His other interest is the total energy and molecular orbital analysis of the chemisorption and reactivity of small molecules on metal, alloy, oxide, and sulfide surfaces. He is now "Directeur de Recherche" at CNRS and "Maître de conférence" at the "Ecole Polytechnique".

I. Introduction

From the inception of scanning tunneling microscopy, the precise interpretation of the atomic scale images has always been a concern and a problem. This stems from the fact that the image is not at all a steric representation of the surface but is a view of its electronic structure at the Fermi level energy. In most cases, it is therefore not possible to directly and simply relate the bumps and shapes on the STM image to the actual lateral positions of atoms. Identifying the nature of the atoms or their heights above the surface is an even greater challenge. Our discussion will be limited here to the case of images of adsorbates on a surface, atoms, or molecules. Such adsorbates clearly give a perturbation of the electronic structure and STM current in their vicinity compared to the bare surface, resulting in specific patterns in the image that are independent if the adsorbates are sufficiently isolated from each other. The shape and amplitude of these patterns cannot be easily related with the nature and structure of the adsorbate, especially in the case of molecules. The well-known counterintuitive example is the case of atomic oxygen chemisorbed on a metal surface, which appears as a depression in the STM image even if the atom is positioned above the metal surface layer. The influence of the nature of the substrate and of the chemisorption site and geometry of the adsorbate is also not clear. Moreover the height of the pattern in a topographic image is generally much lower than the real height of the adsorbate. In relation to the electronic structure of the adsorbate, it would also be important to determine which electronic states or orbitals predominantly contribute to the image contrast. The implication for the image of changes in the surface structure, such as adsorbate-induced relaxation and reconstruction effects, is not well understood.

In the case where the adsorbate is present on the surface in the form of a dense layer, additional questions arise. Indeed, the shapes induced by the adsorbates are no longer independent since they will "overlap" to yield the final image. How the image will change with coverage is therefore not clear, especially in the case where the adsorbates adopt inequivalent positions on the surface.

Moreover, the STM has technical characteristics that can also influence the contrast. The main one is the probe tip whose apex structure and nature is generally not at all well defined, and even changes in the course of an experiment. It is obvious that the tip apex is a direct partner in the tunnel process and, as evidenced by experiments, that its structure can influence the resulting image. In addition, the tip can even directly modify the adsorbate itself by

S0009-2665(96)00082-9 CCC: $28.00

application of a force: molecules can be displaced on the surface in which case imaging is problematic, or they can be distorted which will modify the contrast. Finally the applied bias voltage between tip and surface is an important parameter which opens the way to spectroscopic approaches.

This paper reviews theoretical calculations that can bring insights to these open questions when imaging adsorbates on a substrate.

II. Theories for the Simulation of STM Images of Adsorbates

General theories for STM image calculations can directly be applied, in principle, to the case of adsorbates, even if large adsorbates cannot be handled by all methods due to computer limitations. It is not the purpose of this section to give a systematic presentation of all calculation methods but to make a brief presentation of the main classes of methods and to underline the essential points necessary for the following discussion.

The knowledge of the electronic structure of the system consisting of surface and tip is a prerequisite for the calculation of the tunneling current. Therefore, it is important to separate the approximations made in the treatment of the Hamiltonian from those used for the calculation of the current. For the electronic structure, various levels of approximation are used ranging from effective Hamiltonian approaches like extended Hückel,[1] to first-principles self-consistent methods based mainly on the density functional theory.[2]

Various levels of approximation are also used for the calculation of the current. The most popular class of methods relies on perturbation theory, following Bardeen,[3] and Tersoff and Hamann.[4−6] One advantage of this approach is that, assuming an s-wave for the tip, the current can be related to a property of the surface alone: it is proportional to the local density of states (LDOS) at the center of curvature of the tip and for the Fermi level energy. It is important to underline the difference between this quantity and the total charge density at the same position which can be probed for example by He scattering. The interpretation of the *total* charge density for He scattering is rather easy since an isocontour follows the van der Waals shape of the surface atoms. This is completely different from STM which, in the previously described approximation, is considered as a probe of the charge density for the electronic states at the Fermi level only and not for all occupied states. This explains, in simple terms, the general difficulty in understanding STM images.

This approach is based on several important approximations.[7] The tip and the surface are treated separately, which neglects any interaction between them and is valid only in the limit of large tip−surface distances. Secondly, a severe approximation is made to the structure of the tip apex and any tip dependence of the image is lost. Chen has generalized the perturbation approach[8,9] to p and d states as tip orbitals, by calculating the corresponding tunneling matrix elements.[10] Tsukada et al. have extended the perturbation approach to a more precise description of the structure of the tip than a single atomic state,[11] and have introduced an accurate description of the wave function tail in vacuum.[12] In this approach, the tip apex is described by a cluster of ∼10 atoms and the dependence of the image on the tip structure can be explored.[13]

The second class of methods goes beyond perturbation theory by a proper description of the interacting sample and tip with a scattering theory formalism. The basic idea is to consider the tunnel gap as a two-dimensional defect inserted between two semiinfinite periodic systems. The tunnel event is then viewed as a scattering process: incoming electrons, for example from the bulk of the sample, scatter from the tunnel junction and have a small probability to penetrate into the tip, and a large one to be reflected toward the bulk. The channels for scattering are hence the asymptotic wave functions for the bulk of the sample and of the tip, far from the tunnel junction. Multiple scattering events in the barrier are here taken into account, which as shown by Sacks and Noguera[14−16] are the key difference with respect to perturbative approaches. In this case, the current has been shown to be strongly dependent upon the chemical nature of the tip, even if a s-wave is assumed, if rather short distances are considered between the tip and the surface. Tip-induced localized states, characteristic of covalent (or ionocovalent) partial bond between the electrodes, are present as shown by Ciraci et al.[17,18] Barrier resonances play also an important role in the conductance.[19,20]

Among this second class of methods,[21−23] some have been especially applied to the case of adsorbate imaging and will be briefly introduced here. Doyen et al. developed a method based on a layer Green function formalism.[24,25] A model Hamiltonian approach is used for the description of the tip, consisting of a single atom (e.g. W, Al) adsorbed on a metal surface. Sautet and Joachim have adopted the scattering matrix approach and the generalized Landauer's theory to calculate the tunnel current, in their electron scattering quantum chemical (ESQC) approach.[26] The system for the calculations is infinite in the direction perpendicular to the surface, the tunnel junction being modeled by the approach of substrate and tip semiinfinite bulk solids. The adsorbate is chemisorbed on the substrate surface, while the tip apex, attached to the second semiinfinite solid, is modeled by a cluster of 1−15 atoms. Coupling with the tip and substrate electron reservoirs is hence fully taken into account. The Hamiltonian matrix elements on an orbital basis set, which are the ingredients of the scattering matrix calculation, are obtained with an effective Hamiltonian approach, the extended Hückel theory. Images are generally interpreted in terms of quantum interference effects between different electron tunneling channels.

Kenkre, Biscarini, and Bustamente (KBB) approached the tunnel current calculation as a transport problem in quantum statistical mechanics and incorporated thermal effects and reservoir interactions.[27,28] They are able to describe an arbitrary degree of quantum coherence in the tunnel junction. They especially underline quantum interference effects and apply their theory on the basis of an extended Hückel electronic structure theory.

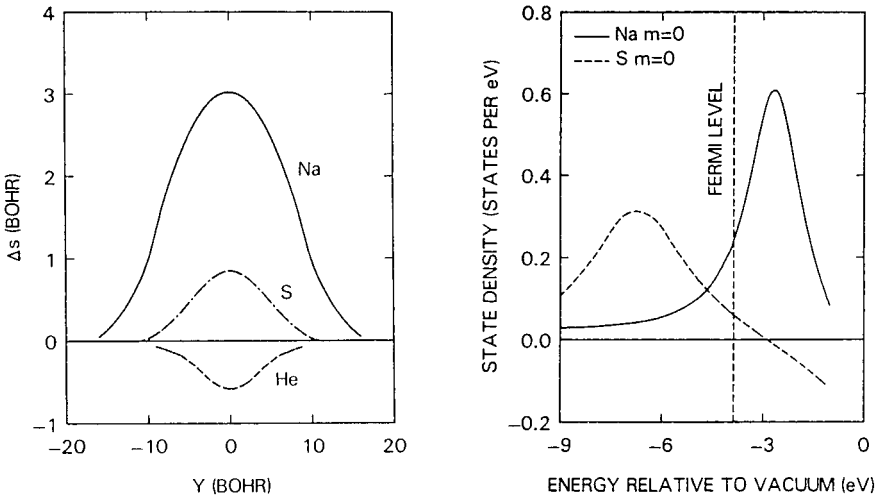

Figure 1. (a) Tip displacement $\Delta s = s(Y) - s(\infty)$ versus lateral separation Y for constant current with $s(\infty) = 16$ bohrs. Tip atom is Na and sample adatoms are Na, S, He (1 bohr = 0.529 Å). (b) Difference in eigenstate energy between the metal−adatom system and the bare metal for Na and S (Part a and b: Reprinted from ref 31. Copyright 1986 American Institute of Physics.)

III. Isolated Adsorbates

1. Imaging a Single Adatom on a Metal Surface

One important difficulty in STM of adsorbates is to identify the nature of the species that corresponds to the pattern observed in the image. This simply arises from the fact that STM probes the electronic structure of the surface at the Fermi level and is therefore only indirectly sensitive to the position and chemical nature of the nuclei. The simplest version of this problem is to consider atoms adsorbed on a metal surface and to inquire how the associated shape in the image might depend on the chosen element, for example on its electronegativity, electronic radius, polarizability etc. In this section only low bias imaging will be considered and the effect of a finite bias voltage will be addressed later.

The pioneering work in this direction was performed by Lang.[29,30] In his approach, the surface and tip electrodes are described by the jellium model, in which the ionic lattice of each metal is smeared out into a uniform positive charge background. The perturbative approach of Bardeen is used to calculate the tunnel current. The tip apex is described by a Na atom positioned on the tip electrode. Constant current scans of this tip above Na, S, or He atoms yield characteristically different results[31] (Figure 1a). Na and S atoms are imaged as bumps, but the maximum tip displacement is much smaller for S (0.8 bohr = 0.4 Å) than for Na (3 bohr = 1.6 Å). Two reasons are given: S sits closer to the surface than Na and the Fermi level state density for S is smaller than that for Na (Figure 1b). For the He, the tip displacement is slightly negative (−0.6 bohr = −0.3 Å) which means that the atom would be imaged as a depression. The valence shell of He (1s) is very low in energy, and its only effect is to polarize metal states away from the Fermi energy, yielding a decrease of the state density near that energy compared to the bare metal. A small electronegative atom like oxygen would also make a negative contribution to the total state density at the Fermi level and produce a depression[32] (−0.2 bohr = −0.1 Å). In this study, the actual value of the tunnel current (or the tunnel conductance) is not determined in an absolute way. The "relative current" value, to be kept constant in the scan, is obtained with a chosen height difference of 16 bohr (= 8.5 Å) between tip atom and adsorbate atom and with an infinite lateral displacement of those two atoms. Since the tip−sample distance is generally not accessible from the experiments, a direct comparison of the calculation results with measured corrugations (at a given tunnel gap conductance) is not possible. For a C adsorbate the depression is 0.15 Å deep for an initial height difference of 8.5 Å and increases to 0.3 Å if the separation is reduced to 5.3 Å.[33] The same interpretation is given for the depression as in the case of the O atom, despite the significantly reduced electronegativity. Another limitation is that the chemical nature and atomic structure of the metal surface are not taken into account, so that arguments such as binding site of the adatom cannot be addressed. The tip displacement curve was shown to correspond to the contour of constant local density of states *at the Fermi level* in agreement with the discussion by Tersoff and Hamann in the case of an s-wave tip. Such an agreement is not surprising here since a Na atom, with dominant 3s character, was chosen as tip atom. However, the tip displacement is noticeably different from the profile of the total charge density as explained previously.

The case of the rare gas Xe adatom is interesting since the adatom shows a high 1.5 Å bump in the STM image on Ni(110),[34] although Xe, like He, would seem to have no electronic states in the proximity of the Fermi level. It was shown with Lang's approach that the measured tip trajectory is close to a contour of constant local density of states at the Fermi level and that the main contribution comes from the tail of the Xe 6s resonance. This resonance is located almost 4 eV above the Fermi level, but this is compensated by the extended radius of the 6s orbital and by the fact that physisorbed Xe binds at a large

distance from the surface. Bouju et al. have addressed the same problem with ESQC.[35] An atomic description of the Cu(110) substrate and Cu tip is used. The calculated image shows a combination of the 0.17 Å corrugated rows of the Cu(110) substrate and a slightly elliptic ∼1.7 Å high bump for Xe in good agreement with Eigler's data and with the previous calculations. Another approach of rare gas imaging was proposed by Mahanty et al.[36] It was shown that the tunnel potential barrier height is significantly reduced in the region above the atom. This was explained by the self-energy of the tunneling electron from the induced polarization of the atom. The enhancement of the tunnel current depends directly on the effective polarizability of the adsorbed species.

The question of the pattern produced by an oxygen atom on a metal surface has also been addressed by Doyen and co-workers with a model Hamiltonian study on Ni(100).[37] Tip and sample are treated on equal footing and the tip consists of a tungsten atom chemisorbed on a flat W(110) surface. The equilibrium distance of O on Ni(110) was calculated to be 0.9 Å above the first layer of Ni atoms, in good agreement with experimental structure, and adsorbed oxygen shows an increased spatial extension due to the partial filling of the 3s affinity orbital. The perturbative transfer Hamiltonian approach is used to calculate the tunnel current. The results contrast with that of Lang and depend on the chosen tip−surface separation on the clean metal. The adatom is calculated as a bump for a separation larger than 7 Å (a bump of 0.4 Å height for 8 Å separation) and is almost invisible for separations between 6 and 7 Å. Only for an even smaller separation would the oxygen atom appear as a dent in the scan. Such an effect is not shown in the experimental data where the O atom is imaged as a depression in a large range of separations.

One important point is that the contours of constant tunnel current show in these calculations a behavior different from those of the Fermi level charge density, which would indicate a rather large bump shape for the adatom for all physically reasonable tip−surface separations. This reveals a breakdown of the Tersoff−Hamann hypothesis. The given reason is that the adsorbed oxygen atom strongly perturbs the exponential decay of the Ni wave function. Moreover due to the diffuseness of the W atom, the amplitude of the sample wave function is not probed at the center of the tip but predominantly 2−4 Å closer to the surface, probing somewhat into the interior of the surface. It is important here to comment on the description of the decay of the metal wave function away from the surface. In Doyen's calculations, the potential is described as a step function, which yields a considerably faster decay of the eigenfunctions than the jellium model.[38] The contribution of the adatom in the wave functions will therefore be more important, yielding a higher protrusion. A correct description of the decay of the metal wave function thus appears to be a crucial point. A simple test in that respect would be to calculate the tunnel current as a function of tip−surface separation and to compare with experimental results. Another reason for the discrepancy could be a slightly exaggerated spatial extension of the O atom in the spin unrestricted Hartree−Fock calculations of Doyen.

A study of O imaging on Al(111) has been performed by Jacobsen et al.[39] with a Tersoff−Hamman approach and density functional calculations. Oxygen is imaged as a rather deep depression (∼1 Å) with a small protrusion in the center. However the minimum tip height in the isocontour of LDOS corresponds to a separation of ∼1 Å compared to the O adatom, which seems somewhat small. C on Ni(100) has been calculated by Hörmandinger et al.[40] with a method based on Bardeen's approximation and a Green function formalism. For the quasi-isolated adatoms in a p(3×3) arrangement, C appears as a only 0.08 Å deep depression for tunneling conditions of $I = 1$ nA and $V_{sample} = -0.5$ V. As did Lang, this is interpreted as a carbon-induced depletion of the surface local state density.

Biscarini and co-workers have also addressed this problem of the STM contrast of adatoms with their KBB approach.[41] The authors have considered Au, Na, H, C, and O on a Au(111) surface described by a cluster in most cases built from a single layer of atoms. For a current of 1 nA and a bias voltage of 20 mV, an Au adatom appears as a 2.45 Å protrusion while Na appears as a 3.5 Å bump, much higher than the 1.6 Å value of Lang. For H, the pattern depends on the tip−sample distance: a hole for 4 Å and a small bump for 5 Å. This effect of H appearing smaller is interpreted by its closer distance to the surface and also by the low-energy position of the H adatom resonance compared to the Fermi level. A similar inversion of contrast with tip−surface separation appears for C: a protrusion for $z = 4$ Å and a depression for $z = 3.5$ Å. The oxygen atom is imaged as a depression with no contrast inversion when the tip substrate separation is increased. However, topographic values are not given. The depression, called "non topographical feature" by the authors is related to resonance in the adatom for energies below the Fermi level and to an interference occurring between direct tip−substrate and adsorbate-mediated tunneling.

One striking aspect of this study is that the corrugation obtained for Na is much larger than the result of Lang and that the considered tip−surface separations are much smaller than Lang's and Doyen's (4−5 Å compared to 8 Å or more). The purpose of Biscarini et al. is primary qualitative, but as they have remarked, the decay of the wave function and current as the tip is moved away from the surface is too fast in their calculations (more than 2 orders of magnitude when the tip is retracted by 1 Å). This decay is much stronger than that observed experimentally (close to 1 order of magnitude of current per angstrom), and this explains why the tip has to come near the surface in order to reach a reasonable current and also why the adatom protrusion is higher. The effect is similar, but stronger, to that for the comparison between Lang's and Doyen's results.

The fast decay of the current can be attributed, as will be discussed later, to the choice of single-ζ orbital

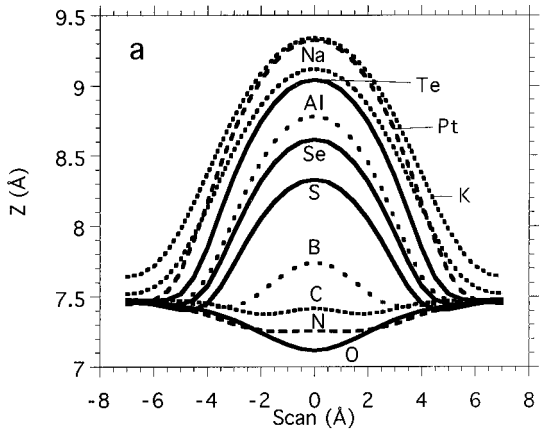

Figure 2. Topographic profiles of atomic adsorbates for a tunnel current of 1 nA and a bias voltage of 10 mV. *Z* is the distance between the tip apex atom and the first Pt layer, and the scan is centered on the adsorbate. (Reprinted from ref 42. Copyright 1997 Elsevier.)

functions for the s and p orbitals of Au. Such single-ζ orbitals are well adapted to describe the short-range interaction between two neighbor atoms in the solid, but they are too contracted to correctly describe the long-range interaction between tip and surface atoms.

More recently, a study of adatom contrast with the STM by Sautet has appeared.[42] The ESQC approach is used to calculate the current in a low bias voltage approximation on the basis of extended Hückel Hamiltonian matrix elements. The image of several atoms (see Figure 2) is studied on a Pt(111) surface with a Pt tip (the tip apex is a Pt tetrahedron connected to the tip base). In contrast with to the previous paper, double-ζ functions[43] are used to describe all atomic functions in the tunnel gap region. Only selected elements will be discussed here and compared to previous studies and experiment. If a set point current of 1 nA and a bias voltage of 10 mV is assumed, O appears as a −0.35 Å deep depression, significantly lower than Lang's result (−0.1 Å) and in good agreement with experiment (−0.3 Å). Sulfur is calculated as a protrusion of 0.8 Å height (Lang 0.4 Å) and Na as a 1.7 Å high bump (Lang 1.6 Å). A recent experimental study of isolated S atoms on Pd(111) gives a 0.85 Å bump for S. Although the relative corrugations agree well between calculations, absolute values of the corrugation are somewhat larger than that given by Lang. Two causes can be proposed to understand the difference. The first one is the tip−surface separation far from the adsorbate. Lang uses a 8.5 Å separation between tip atom and *adsorbate* atom. The value obtained by Sautet for a 10 MΩ gap resistance is 7.5 Å between tip atom and *metal* surface, which for a S adatom for example would reduce to ∼6 Å between tip atom and adsorbate atom explaining the larger corrugation values. Secondly the tip apex is different. The decays of the tunnel current as a function of tip−sample separation are rather similar (0.9 order of magnitude current per angstrom (Lang) compared to 0.98 (Sautet)). The main limitation of Sautet's calculation is the semiempirical non-SCF description of the electronic structure, while Lang's approach neglects the atomic

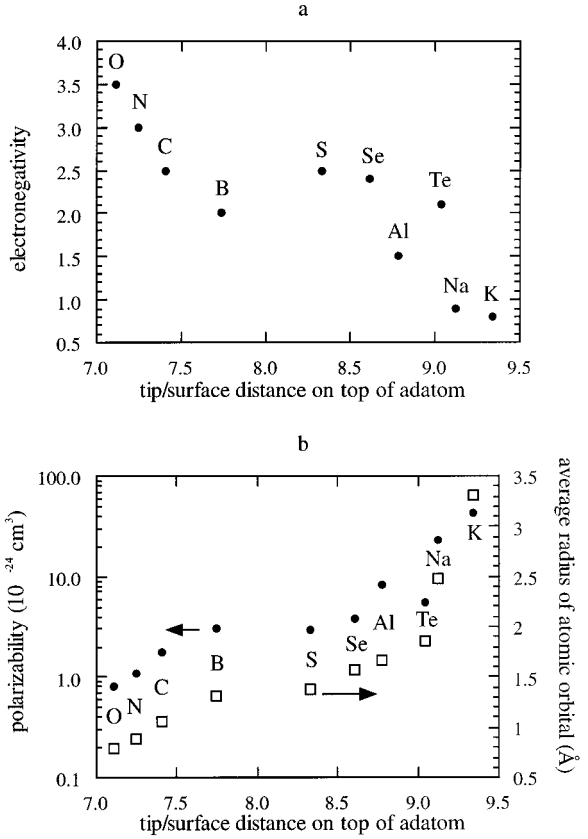

Figure 3. Correlation between the tip height on top of the adsorbate and (a) the atom electronegativity or (b) the atomic polarizability and the average radius of the most important atomic orbital. (Reprinted from ref 42. Copyright 1997 Elsevier.)

structure of the substrate and relies on a perturbative treatment for the current calculation.

Correlations drawn between adatom STM corrugation and elemental electronegativity or polarizability are shown in Figure 3. The correlation with electronegativity, often presented in the discussions, is only partly correct since elements with the same electronegativity, like C and S, can give a very different pattern. The comparison with polarizability is more satisfactory which means that the electronic radius of the atomic orbitals is the key factor that controls the tunnel response of the adsorbate, the energy position of the orbital playing also a role but less important. An analysis of the adatom STM shape is proposed on the basis of a decomposition of the electronic interaction through the tunnel gap. The interactions between tip and metal surface atoms are responsible for the tunnel current far from the adatom and this through-surface contribution to the tunneling amplitude is decreased in the vicinity of the adatom due to the shift in energy of the surface levels induced by chemisorption. In addition, the tip interacts with the adsorbate itself and the current that would result from this interaction alone is called the through-adsorbate current. The final current results from constructive or destructive interferences between the through-adsorbate and through-surface tunneling amplitudes. The through-adsorbate contribution to the current has a bump shape and decays away from the adsorbate. The maximum value of this bump, compared to the through-surface current, mainly depends on the orbital extension and controls

Table 1. Apparent Height (Å) of Adatoms in STM Images from Different Theoretical Approaches[a]

	Lang[29−34]	Doyen et al.[37]	Hörmandinger et al.[40]	Biscarini et al.[41]	Sautet[42]	experiment
O	−0.1	−0.2/+0.4			−0.35	∼−0.3[b]
C	−0.15/−0.3		−0.08	+0.55/−0.7	−0.1	+0.3/−0.3[33,79,80]
S	0.4				0.8	0.85[c]
Na	1.6			3.5	1.7	
Xe	1.7				1.7	1.5[34]

[a] Negative values indicate that the adatom appears as a depression. [b] Eigler, D. Unpublished results. Esch, S.; Hohage, M.; Michely, T.; Comsa, G. *Phys. Rev. Lett.* **1994**, *72*, 518. Brune, H.; Winterlin, J.; Behm, R. J.; Ertl, G. *Phys. Rev. Lett.* **1992**, *68*, 624. Brune, H.; Winterlin, J.; Trost, J.; Behm, R. J.; Ertl, G. *J. Chem. Phys.* **1993**, *99*, 2128. Ruan, L.; Besenbacher, F.; Stengaard, I.; Laegsgaard, E. *Phys. Rev. Lett.* **1993**, *70*, 4079. Kopatzki, E.; Behm, R. J. *Surf. Sci.* **1991**, *245*, 255. [c] On Pd(111) from Rose, M.; Behler, S.; Salmeron, M. Unpublished results.

the final image shape. For a contracted atom like oxygen, the through-adsorbate current is small and the depression in the through-surface contribution imposes the final dip shape. Carbon is a frontier element since through-adsorbate and through-surface contributions have the same magnitude which results in a weak contrast. The more polarizable S atom gives a large through-adsorbate current and the final image is a bump.

The through-adatom current can be further decomposed into interfering atomic orbital contributions, which originate from tails, at the Fermi energy, of resonances from adatom atomic levels (nonresonant tunneling).

The comparison of these different studies, summarized in Table 1, therefore gives a rather coherent picture of the imaging of adatoms with the STM. The various and complementary interpretations enable a qualitative understanding of the adatom contrast, the shape of which constitutes a "chemical fingerprint" of the adsorbate.

2. Images of Molecules

Compared to atoms, the interpretation of the contrast of chemisorbed molecules adds a level of complexity. Similar questions arise such as the general aspect (bump or hole) or the corrugation of the features but specific additional problems appear. In many cases, the pattern shows internal structures and details, but for molecules it is not clear at all what the bumps mean and even whether they are located on some atoms of the adsorbate. However, this molecular resolution image contains information that needs to be related to the electronic structure of the molecule, in order to establish a correspondence between the observed pattern and the chemical nature of the molecule. Moreover, molecules can adopt different coordination modes and binding sites at surfaces and the dependence of the STM image on these geometrical factors needs to be clarified.

One of the simplest molecules studied with STM is CO. When chemisorbed on a Pt(111) surface and imaged at very low temperature (4 K) to avoid mobility, CO shows two different images[44,45] (Figure 4). One can be described as a bump with a height of 0.44 Å while in the second image the bump is lower (0.14 Å) and is surrounded by a circular depression (∼−0.1 Å). These two different shapes are not due to different imaging conditions, such as bias or different tip apex structure, since they can be found together in the same image, but have been attributed to two different chemisorption sites of the molecule

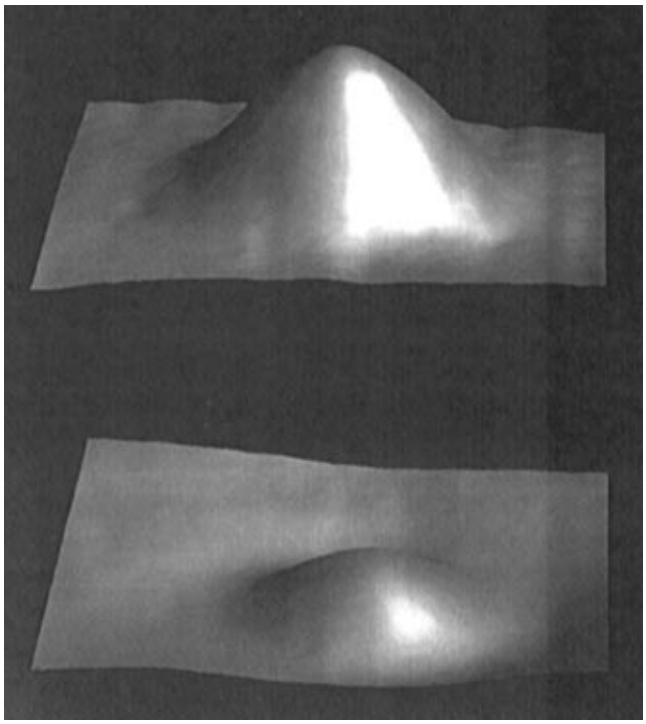

Figure 4. Two 10 Å × 10 Å STM topographic images of the CO molecule on Pt(111) obtained by Eigler et al. (bias = 0.01 V, current = 1 nA). (Top) "Bump"-state CO, 0.44 Å high. (Bottom) "Sombrero"-state CO; the peak of the protrusion is 0.14 Å above the Pt plane and the moat around it is 0.07 Å deep. (Reprinted from ref 44. Copyright 1991 Science American Association for the Advancement of Science.)

on the surface, presumably top and bridge chemisorption sites. Notice that it was not possible to identify these binding sites from STM alone, since the short tip−sample distances necessary to resolve the substrate generally displaces the molecules. Therefore only the relative registry of the two molecular features can be obtained after calibration of the piezoscanner. This problem is rather general for STM imaging of molecules. Therefore theoretical simulations can be of great value here in explaining the site dependence of the pattern and identifying the binding site.

Images of CO on Au(111) have been calculated by Biscarini et al.[41] with their approach (KBB). At the top site, CO appears as a 2 Å high protrusion, while the bridge site gives a somewhat lower feature (1.8 Å). Even if the qualitative comparison between top and bridge sites seems correctly described, the size of the bumps is overestimated and this can be associated, as in the previous section, with the too rapid decay in vacuum of the metal wave function.

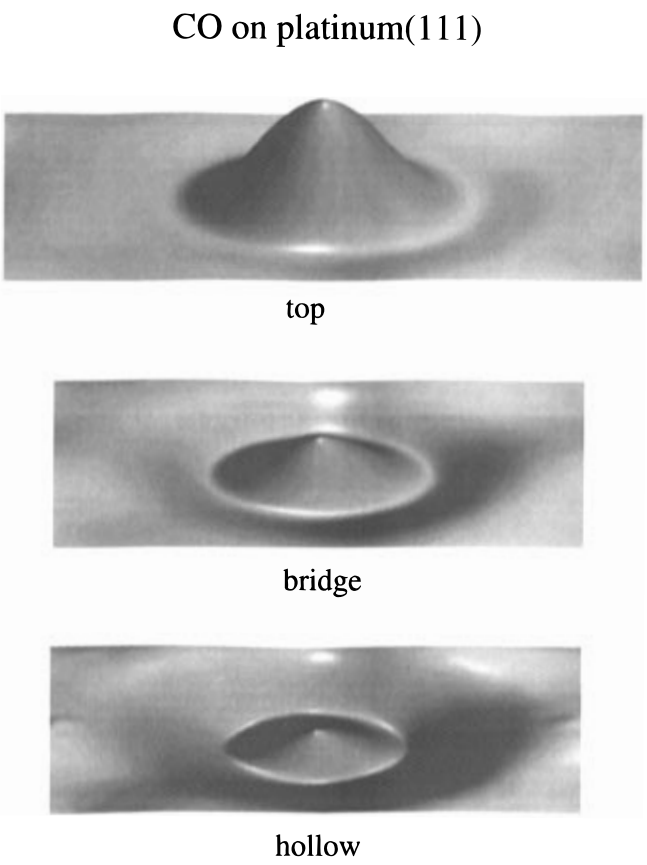

Figure 5. Calculated topographic images for CO on Pt-(111) (bias = 10 mV, current = 1 nA): (top) on-top site (16.6 Å × 12 Å, *z* range = 0.47 Å); (middle) bridge site (13.8 Å × 12 Å, *z* range = 0.18 Å, including a 0.08 Å deep depression); (bottom) hollow site (13.8 Å × 12 Å, *z* range = 0.1 Å). (Reprinted from ref 46. Copyright 1996 Elsevier.)

A second study was presented by Bocquet et al.[46] with the STM-ESQC approach on a Pt(111) substrate. The calculated images are shown in Figure 5. The top site result is in very good agreement with the first experimental shape while the bridge calculated image closely resembles the second "sombrero" shape. The authors showed that despite the semiempirical treatment of the wave function, the image corrugations, and shapes are reproduced in a semiquantitative way. The hollow site, not present in the experiment, is predicted to give a smaller bump surrounded by an even deeper depression. So when going from top to bridge and then to hollow site, the image changes as if the molecule bump was pushed down to lower *z* values, causing a depression around it. A simple interpretation is proposed for this evolution of the image shape (see Figure 6). It is based on a decomposition of the current similar to that used for the images of adatoms. The "through-space" current, resulting from the interaction between tip and surface metal atoms, is weakened in the region of the admolecule and this in a similar way for both sites. Moreover, the tip−molecule electronic interaction results in a "through-molecule" current which image is a bump located on the molecule, decaying to zero when the tip is moved away. The final contrast is given by the superposition, with interference effects, of these two current contributions. In the case of the top site, the through molecule bump is strong enough to cancel the depression in the through-space component. For the bridge site, the through-molecule contribution is reduced, mainly because the molecule sits at a lower *z* on the surface: the bump moves down and the through-space depression is no longer completely compensated. An additional point in the discussion describes the contribution of CO molecular orbitals to the through-molecule current. It is shown that, due to the perpendicular orientation of the molecule, π_{CO} and π^*_{CO} bonding and antibonding orbitals have a very small influence, the current being dominated by the 5σ lone pair contribution. This contribution is however not very strong, due to the contracted nature of the O atomic orbitals and their small contribution in the 5σ MO, and this explains the weak final contrast of the molecule (0.45 Å for top site) despite the fact that the O end of the molecule is 3 Å above the surface.

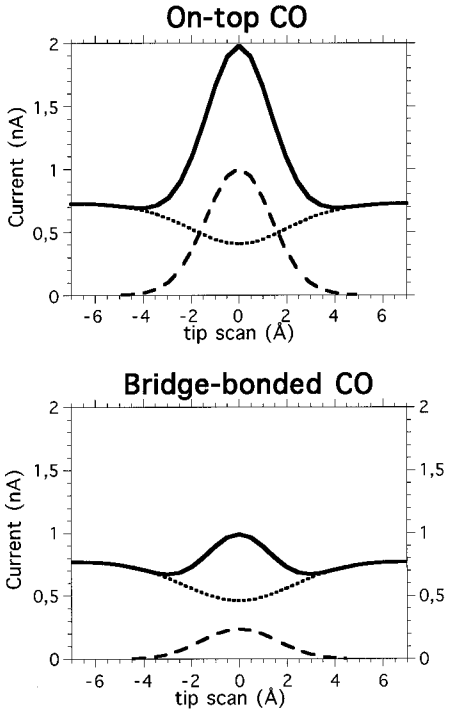

Figure 6. Contributions to the tunnel current for top and bridge site CO on Pt(111): the through-molecule (TM, dashed line) current and the through-space (TS, dotted line) current interfere to give the final contrast (solid line). A constant height scan centered on the molecule is represented. The tip height relative to the surface is 7.5 Å and the bias voltage is 10 mV. (Reprinted from ref 46. Copyright 1996 Elsevier.)

Physisorption of small organic molecules on graphite was studied with a quantum chemical approach by Lambin et al.,[47] with the aim to understand how STM imaging can depend on the nature of chemical groups present in a molecule or polymer. Graphite was modeled by a benzene molecule and physisorption of CH_4, H_2O, H_2S, CF_4, and benzene was studied at the Hartree−Fock level, with special emphasis on the top valence electronic levels[48,49] and on the influence of an electric field. The tunnel current was not explicitly calculated but qualitatively related with the electronic structure. The highest occupied molecular orbital (HOMO) of the complexes always correspond to the HOMO of the benzene "substrate", the MO's localized on the molecule being very far in energy for CF_4, intermediate for CH_4 and H_2O, but

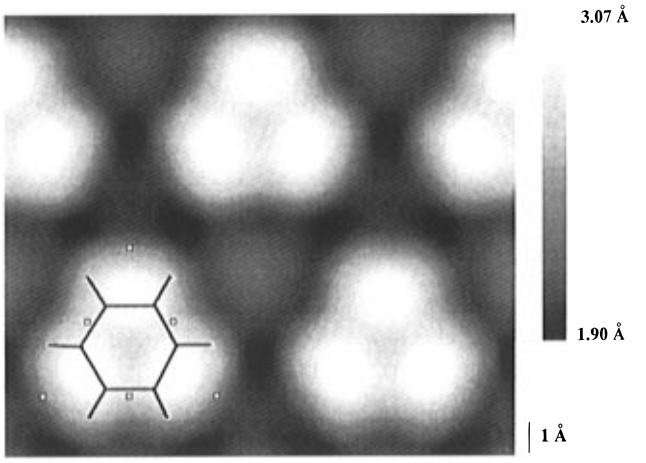

Figure 7. Calculated topographic STM image of benzene on Rh(111) (current 2 nA, voltage 10 mV). A stick model of one of the benzene molecule is given, and the neighboring Rh atoms are indicated by white squares. The origin of the *z* scale (in Å) is arbitrary. (Reprinted from ref 63. Copyright 1992 Elsevier.)

very close in energy for the S3p level of H_2S and obviously for the benzene dimer. In the case of H_2S, a relatively strong interaction occurs with one S3p state, and the HOMO of the complex acquires a significant contribution on that orbital. The two complexes (benzene/H_2S and benzene/benzene) that give rise to a significant interaction correspond to the chemical group (SH and phenyl) that yield a strong response in the STM. The effect was shown to be amplified by the influence of an external electric field.

Among hydrocarbon molecules,[50] the favorite one for STM imaging and calculations is certainly benzene. One of the early experimental images of this molecule, coadsorbed with CO on Rh(111) was obtained by Ohtani et al.:[51] the molecule appears as three lobes arranged in a triangle. The *z* corrugation of the molecule pattern is 0.5−2.0 Å, depending on the imaging conditions. The first calculation of benzene STM image[52] was performed on Rh(111) by Sautet et al. with ESQC (the coadsorbed CO molecules were not included). The calculated image (Figure 7) shows three lobes and the overall shape (lobe separation = 2.7 Å) and corrugation (1.2 Å) are in good agreement with the experiment. The structure of the chemisorbed molecule was taken from LEED:[53] it sits in a 3-fold site on the trigonal Rh(111) surface (a chemist would describe it as a triple $\eta^2\mu^1$ coordination on three neighbor Rh atoms) resulting in a small Kekulé distortion. The lobes in the calculated images are located near the middle of the longer C−C bonds, in between underlying Rh substrate atoms. Hence the STM image of benzene does not show atoms but some of the C−C bonds and the pattern is 3-fold symmetrical. It is important to understand the origin of the lower symmetry of the STM image compared to the gas-phase molecule. It was shown that the image is not significantly changed if the Kekulé distortion is removed, that is if a 6-fold molecule is positioned on the surface. The shape mainly results from the interaction of the molecule with the 3-fold surface site. Benzene does not have any electronic state in resonance with the Fermi level of Rh, the occupied and vacant frontier orbitals being well separated. The contrast was shown to arise from nonresonant tunneling i.e. through tails of molecular orbital resonances. As already noticed for Xe, this is the quasi-general case for the STM imaging of closed-shell adsorbates. For benzene the image shape is governed by the tail of the lowest unoccupied molecular orbital (LUMO) π^*. By interaction with the substrate, this π^* orbital is partially mixed with the HOMO π and this results in the 3-fold shape. The image therefore qualitatively shows how the low-energy antibonding states are deformed and localized by interaction with the surface.[54] The substrate and the symmetry of the binding site therefore have a key importance in the image shape of the molecule.[55] Moreover, the image gives important information on the local reactivity of the molecule on the surface.

The image of benzene on Rh(111) was also calculated by V. Hallmark et al.,[56] this time including the coadsorbed CO molecule present in the 3×3 experimental structure. The result for benzene was qualitatively very similar, and it was also underlined that the presence of a Kekulé distortion was not necessary to produce the three-lobed shape. Biscarini et al. calculated the image of benzene on the hollow site of Au(111) with the KBB approach.[41] In agreement with other calculations, three bright lobes dominate their calculated images; however, the halo surrounding them presents a hexagonal shape, which does not appear in the two previous studies and in the experimental image on Rh. This can be caused by the Au substate, which gives a smaller interaction with the benzene molecule compared to Rh, therefore yielding a less pronouced perturbation of the 6-fold symmetry of the gas-phase molecule or could be attributed to different calculation conditions.

More recently, STM images of isolated benzene molecules have been acquired at very low temperature on a Pt(111) surface.[57,58] One interesting and unexpected point is that, at high resolution, three different characteristic types of protrusions have been found. These images are not related with different STM imaging conditions, but should be associated with different types of benzene molecules on the surface. As in the more recent case of CO discussed above, it was proposed that the three images correspond to different benzene adsorption sites. Such a dependence of the STM image of a molecule on the way it interacts with the surface was already suggested by the benzene on Rh(111) calculations, but was further explored in more detail in subsequent papers.

Images of benzene on graphite and MoS_2 substrates were reported by Fisher et al.[59] with a Tersoff−Hamann approach and an ab initio electronic structure calculation. They underline the sensitivity of the STM image to the molecule−substrate interaction. At low voltage, the STM images a substrate state, modulated by the molecule, and reflects the details of the molecule−substrate interaction. The image then acquires atomic features of the adsorbate, but retains the symmetry of the substrate states. They stress again the importance of substrate-induced broadening of the molecular energy levels into resonances, with a small amplitude tail in the molecule gap and at the substrate Fermi level. As

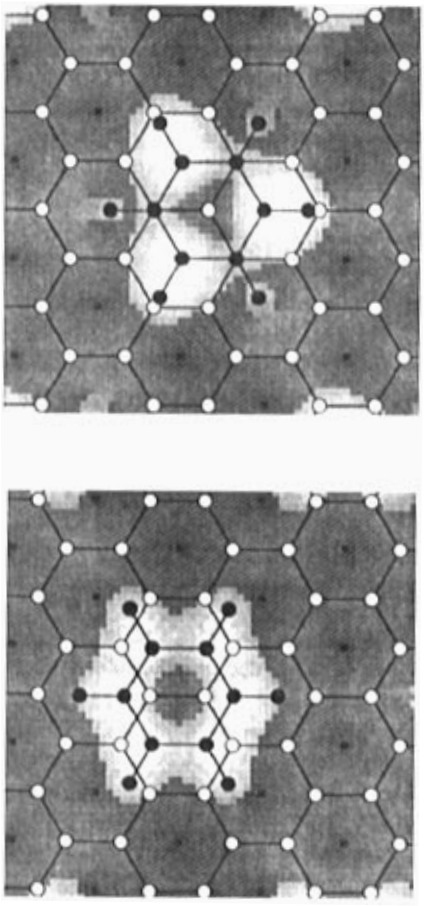

Figure 8. Predicted STM images for benzene on graphite for Fermi level energy (a) 3-fold symmetry site. Atoms above substrate hollows are bright (b) with the benzene ring at a bond centered site with 2-fold symmetry. The gray scale represents the tip height above the surface in constant current mode; filled atoms show molecule atoms, empty atoms substrate atoms. (Reprinted from ref 59. Copyright 1993 American Institute of Physics.)

illustrated in Figure 8 the image of the molecule on graphite is then naturally strongly dependent on the adsorption site. The on-top site shows a 3-fold image, carbon atoms above substrate hollows being brighter. When the molecule is adsorbed on a bond-centered site (Figure 8b), the image is 2-fold symmetric.

The image site dependence for benzene on Pt(111), the experimental substrate of Weiss et al., was studied by Sautet et al.[60] with the ESQC approach. Six chemisorption structures (three sites and two orientations) have been considered. The calculated images strongly depend on the chemisorption site and they allow the assignment of each experimental image of benzene to a given site and orientation of the molecule (Figure 9). The maximum to minimum height differences for a gap resistance of 100 MΩ range between 0.5 and 1 Å, depending on the site and show a good qualitative agreement with the measured values. The hollow site gives an image with three lobes on a triangle, similar to the benzene on Rh(111) case. The top site is associated with a 6-fold volcano shape, which has almost a complete cylindrical symmetry. Finally, the bridge site gives a simple bump shape with only a weak 2-fold aspect. The influence of the molecule−surface distance and of additional adsorption induced deformations of the benzene, such as increase of ring size, Kekulé distortion, and out of plane H tilt, have also been discussed in detail.[61] For the hollow site, a larger radius and tilt angle of the H atoms yield a more pronounced separation of the three lobes with a decrease of the amplitude at the center. A shorter metal−carbon distance also gives an enhancement of the C_3 aspect of the images. For the "volcano shape" on-top benzene, a larger radius gives a greater amplitude of the image, and the best theory−experiment agreement is obtained for a radius of 1.5 Å. Modifying the H tilt angle or the metal−carbon distance changes the relative depth of the crater. The global trend for all sites is that the internal structure in the image, adapted to the symmetry of the substrate, is enhanced when the molecule is more strongly distorted upon adsorption, or if it is adsorbed closer to the surface.

A precise analysis of the molecule contrast was proposed,[62] extending the simple analysis given for benzene on Rh(111).[63] The shape of the pattern and its internal structure is imposed by the through-molecule contribution to the current, but this internal structure is greatly weakened by the interference effect with the through-space current resulting from tip−substrate interaction. The through-molecule current was further decomposed in the contributions (i.e. tails of resonances) of the various molecular orbitals. The main result is that it is not possible to restrict the analysis to the frontier orbitals close to the Fermi level. For example, a calculation including all π orbitals of benzene only would give an image markedly different from the one incorporating the influence of the σ framework.

If a given molecular orbital is chosen, two factors mainly affect the strength of its contribution to the tunnel current. First, an orbital whose energy is close to the Fermi level has a stronger contribution than one which lies far away in energy. However the current decay with the energy difference ΔE is asymptotically proportional to only $1/\Delta E^2$, since the tunnel current resonance has a Lorentzian shape. The second factor is the strength of the electronic couplings of the molecular orbital with the surface and with the tip, the product of which controls the width of the resonance: the current is proportional to the square of this product (Figure 10). One important aspect for these interactions is the number of nodal planes perpendicular to the surface in the MO. In the case of benzene, fully symmetric A_1 orbitals do not have any such nodal plane: their interaction with the tip is favorable and they can give an important contribution to the current, even if they are not so close to the Fermi level. Orbitals with the symmetry of the HOMO have one nodal plane perpendicular to the molecule, and those with the LUMO symmetry have two. The tip overlaps with carbon atoms that have different signs in the MO and the global interaction is weaker. As a consequence, the contribution of these orbitals is smaller, even if they are located closer to the Fermi level.

However, the benzene molecule contrast results from strong interference effects between MO contributions. The most striking interference effect is between σ orbitals built from carbon 2s orbitals, and symmetry associated π orbitals built from $2p_z$. A

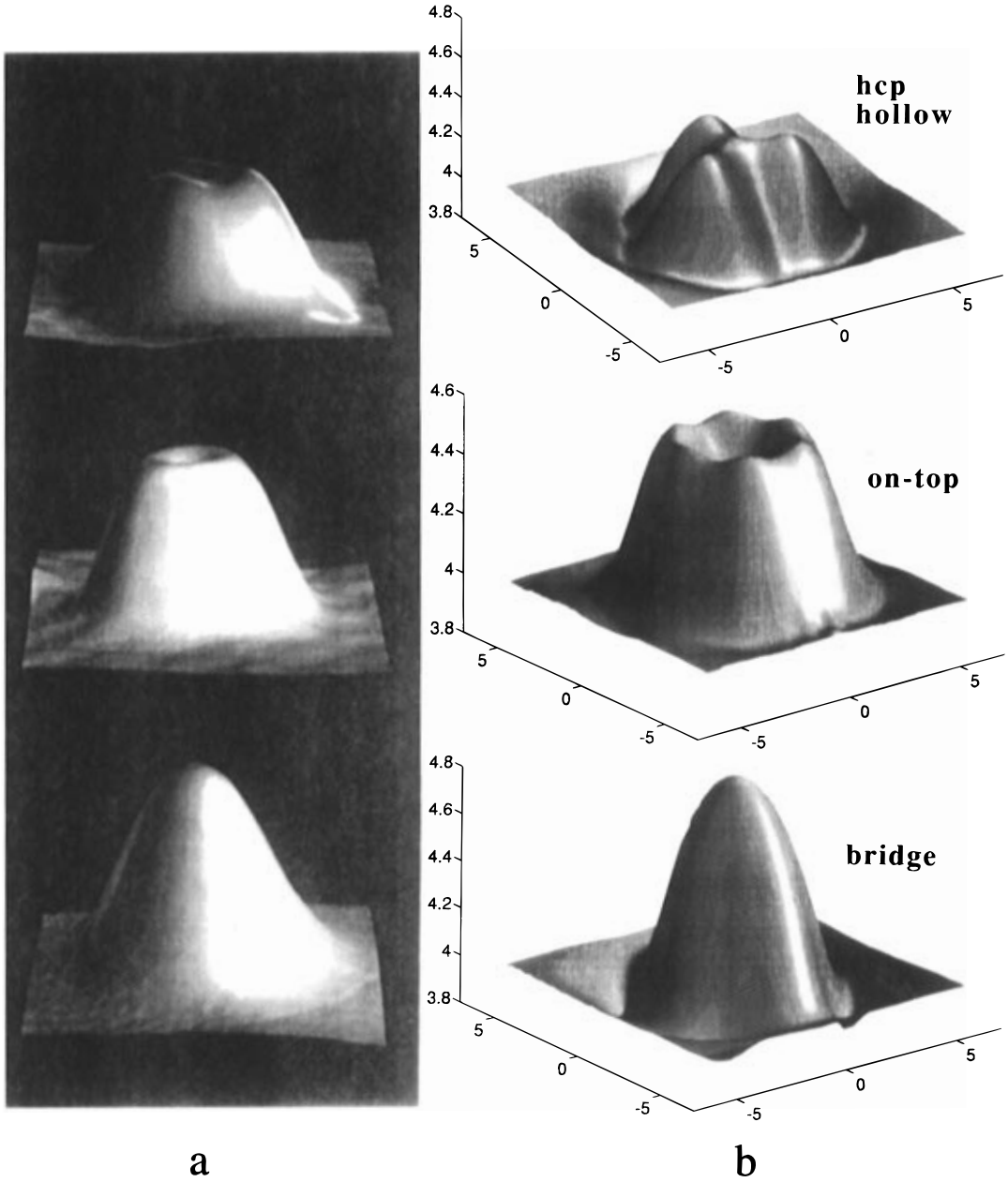

Figure 9. (a) The 3 STM images of the benzene molecule obtained by P. S. Weiss and D. M. Eigler with a gap resistance of 0.1−1 GΩ. The scan size is 15 Å × 15 Å and the image amplitudes are 0.6, 0.7, and 0.9 Å. (b) The calculated topographic images obtained for the chemisorption of benzene on the hollow, on-top, and bridge site with a gap resistance of 0.1 GΩ. The scan size is 12 Å × 12 Å and the image amplitudes are 0.5, 0.65, and 1.0 Å. (Part a: Reprinted from ref 57. Copyright 1993 American Institute of Physics. Part b: Reprinted from ref 61. Copyright 1996 Laser Pages Publishing, Ltd.)

simple analysis, based on the symmetric (anti symmetric) character of s (p_z) orbitals across the tunnel gap, was proposed in order to understand the sign of this $\sigma-\pi$ interference effect. This interference is constructive for the symmetry of the LUMO orbital (E_2), while it is strongly destructive for all other orbital symmetries. This is why orbitals with the LUMO symmetry finally dominate the tunneling process. In the case of the hollow site (with no Kekulé distortion), the 3-fold shape only appears after recombination of MO contributions and arise from the interference between orbitals of LUMO and HOMO symmetries. Therefore, even if for benzene the LUMO orbitals have a large importance in the internal structure, it is not possible to neglect the influence of other orbitals, that are located further from the Fermi level.

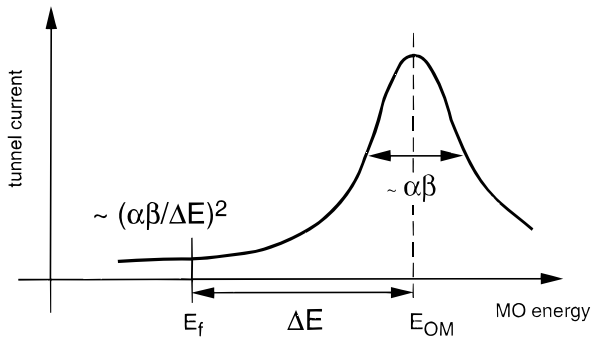

Figure 10. Schematic representation of the lorentzian current resonance associated with a given MO and its tail crossing the Fermi level. The MO−surface electronic interaction is noted α while the MO−tip interaction is noted β.

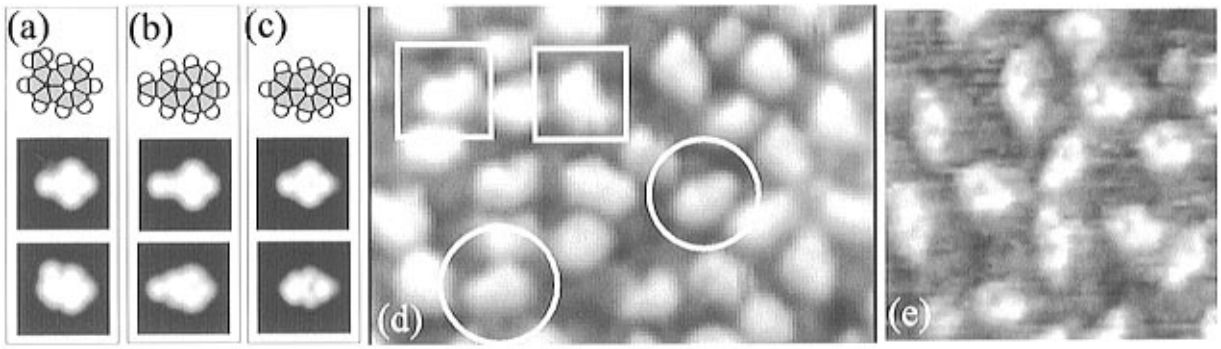

Figure 11. Monomethylazulenes on Pt(111). Schematic, LUMO for isolated molecule (upper plot) and local density of states (lower plot) for (a) 1-methylazulene (1-MA), (b) 2-MA, and (c) 6-MA. Plots for 1-MA and 2-MA are calculated at a height of 2 Å above the molecule, while for 6-MA the height is 0.5 Å. (d) Low-resolution STM image of mixed 1-MA ~20% coverage (in squares, e.g.) and 2-MA (in circles, e.g.). (e) High-resolution images of 6-MA. (Reprinted from ref 64. Copyright 1993 American Institute of Physics.)

Larger unsaturated molecules have also been considered. Images of polycyclic molecules have been calculated by V. Hallmark et al.:[64] naphthalene, azulene, and a variety of substituted azulenes. These molecules have a rather similar structure and the ability of STM to distinguish them in mixed overlayers was demonstrated by a combined experimental and theoretical approach. Even if the calculations of LUMOs and HOMOs for isolated molecules can give some agreement for certain molecules, inclusion of the substrate is required for a correct simulation of the image. The images are then dependent on the adsorbate site symmetry, which needs to be determined either by total energy calculations or by comparison with experimental data. Naphthalene has a bilobal structure, and a double ring pattern can be obtained if a smaller height above the surface is considered for the local density of states calculation. The plot of the isolated molecule LUMO does not agree well with the STM experimental image. The difference between isolated molecule LUMO and LDOS for the chemisorbed molecule is even more striking for monomethylazulene on Pt(111) (Figure 11). Isolated molecule LUMOs do not exhibit significant intensity contributions at the position of the methyl group, implying that the isomers could not be distinguished by STM. The image shapes are however different in the STM data and agree well with the LDOS plots for adsorbed molecules, with intensity on the methyl group position. In this case again, surface-induced mixing between LUMO and HOMO is an important factor for the contrast mechanism. Similar shape recognition was obtained for dimethyl- and trimethylazulene molecules.

The ability of STM to image a large range of molecular adsorbates has been discussed by Ramos[65] with a simple approach based on CNDO molecular orbitals. A projection type criterion was designed in order to calculate the weight of the molecule in the electronic states close to the Fermi level. This enables one to decide whether an STM observation shows the adsorbed molecule directly or the indirect influence of the molecule on the current of the substrate. It was shown that molecules that can be successfully imaged by the STM present a contribution to the wave function greater than 10%.

Even larger molecules have been investigated. Images of Cu−phthalocyanine[66] were calculated by Sautet et al. with the ESQC technique. The interpretation of the contrast mechanism for such large molecules is still an open debate. The molecule appears in the calculated image as a 4-fold arrangement of bright patterns, mainly centered on the carbon atoms, with no protrusion on the central Cu atom. Some internal details are apparent in the image, but they do not correspond to any atomic positions because of the delocalized nature of the electronic structure. The image is built up from the interfering superposition of molecular orbital contributions, which may come from orbitals out of resonance with the Fermi level. More recently images of C_{60} on Au(110)[67] were obtained by Chavy et al. with the same approach. The tunnel current through C_{60} cannot be explained only by the contribution of HOMO and LUMO but tails of resonances from 36 MO's contribute to 90% of this current. The C_{60} apparent height in the image is only 3.5 Å in good agreement with experimental results. An intramolecular contrast is found in the image and this internal shape is dependent on the orientation of the C_{60} molecule (Figure 12). In the equilibrium position (Figure 12, top), the image shows four bumps, which are not located on the top carbon atoms but correspond to the six-member rings. The origin of these four bumps is not straitforward, since it is related with a destructive interference between the C_{60} active tunneling channels when the tip is located on the central bond, creating a depression in the image at that position.

The conclusion that more MO's than only HOMO and LUMO of a molecular adsorbate need to be considered for STM contrast was also underlined in a calculation of STM profiles for adenine on a graphite substrate.[68]

IV. Dense Layers of Adsorbates

The previous discussions were mostly limited to the case of isolated adsorbates. Some ordered layers were considered, but tunneling through single adsorbates was assumed in the image interpretations. Specific effects related with close contact between adsorbates in a dense layer were not addressed. When imaging a dense layer (or a cluster) of adsorbates, the key question is to understand whether the final image will be a simple superposition of isolated adsorbate patterns, or if some more complex process will take place.

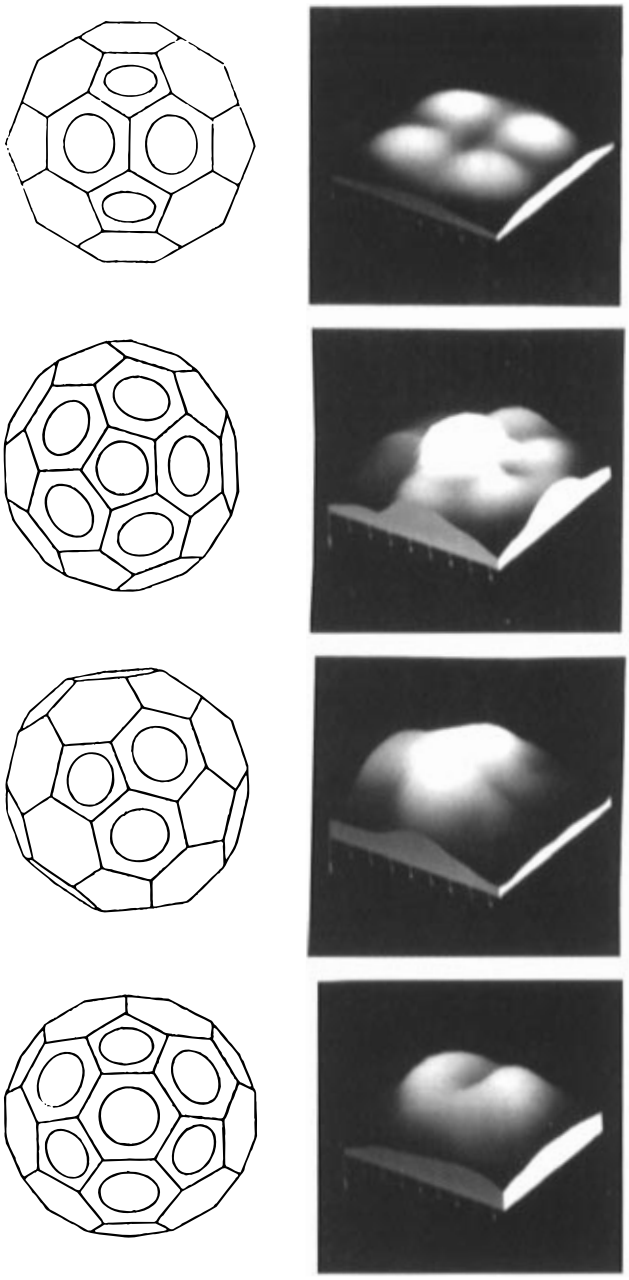

Figure 12. Four 8 × 8 Å^2 calculated constant current STM images of a single C_{60} molecule on Au(110) restricted to the C_{60} top part with a 0.5 Å *z* range from black to white. The C_{60} orientation is different for each image and is drawn on the left as seen from above the surface. The bias voltage is 100 mV and the current is 0.7 nA. (Reprinted from ref 67. Copyright 1993 Elsevier.)

Is the contrast similar in the layer compared to the isolated species? Are the bumps located on all adsorbates? What is the influence of having two types of adsorbates in the layer, with different neighbors? Those are the open questions.

The p(2×2) layer of sulfur on a Re(0001) surface is a simple system well-characterized by surface science techniques, which shows a remarkable tip-dependence effect in STM imaging[69] (Figure 13A). Depending on the tip structure, the sulfur atoms in the layer are imaged as bright balls, triangles, or Y shapes that join to build a honeycomb structure. The calculations[70,71] with ESQC show that the ball shape is obtained with a tip ending with a S atom, the triangle with a Pt termination, and the Y shape with

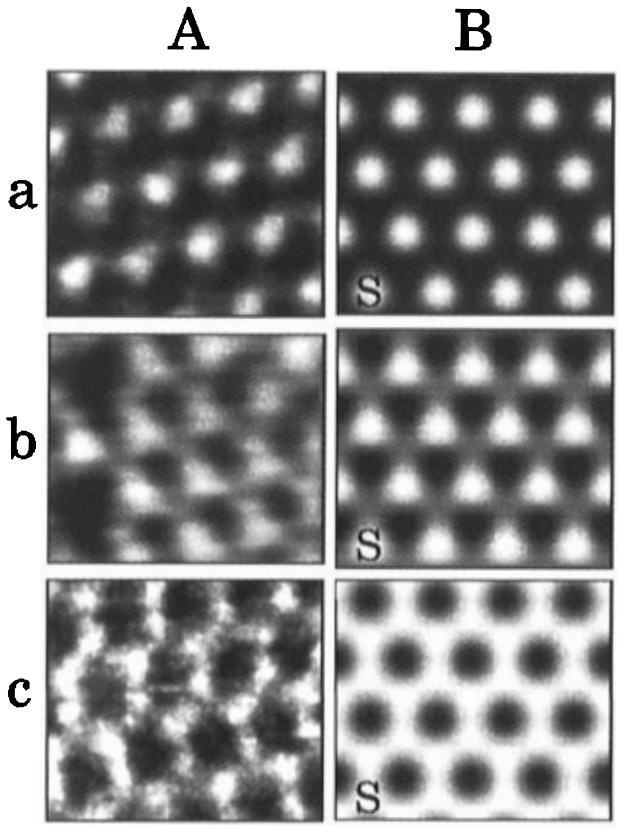

Figure 13. (A) The three experimentally observed STM current images for the (2×2) overlayer of sulfur on Re(0001) at an average gap resistance of 25 MΩ. The shape of the maxima (round (a), triangular (b), and Y-shaped (c)) is not dependent on the bias voltage or gap resistance. (B) Calculated images at the same gap resistance with S atom in the hollow site at a 1.67 Å height and for each selected class of tip represented by tips ending in one sulfur atom (a), one platinum atom (b), or three platinum atoms (c). The position of one sulfur atom is indicated by S. The images are calculated in the constant height mode with a height of the tip matching the experimental gap resistance. (Reprinted from ref 71. Copyright 1993 Elsevier.)

a "flat" tip terminated by three Pt atoms (Figure 13B). More generally, three classes of tips were defined: tips ending with a small main group atom from contamination (e.g. S, C, etc.) would yield the ball shape, those ending with a metal atom (Pt, Rh, Re) give the triangle aspect, while the tip ending by three (or two, respectively) metal atoms at similar distance from the surface give the honeycomb image (or a slightly distorted honeycomb, respectively).

The striking aspect is that all these tip dependence effects disappear if separated atoms are considered.[72] A similar calculation for a fictitious low-density 4×4 layer, where the distance between S atoms on the surface is doubled, gives a ball shape for all types of tips, the only very natural difference being that a larger tip apex would give a larger bump, just by convolution effect. So clearly for that system, there is a strong effect of the dense layer, that switches on the dependence of the image on the tip apex structure. It was shown that in the case of the dense layer the tip can simultaneously overlap with neighboring adsorbates on the surface, which is equivalent to saying that the atomic STM patterns have a significant overlap. The first effect is to reduce the corrugation of the image. A topographic calculation

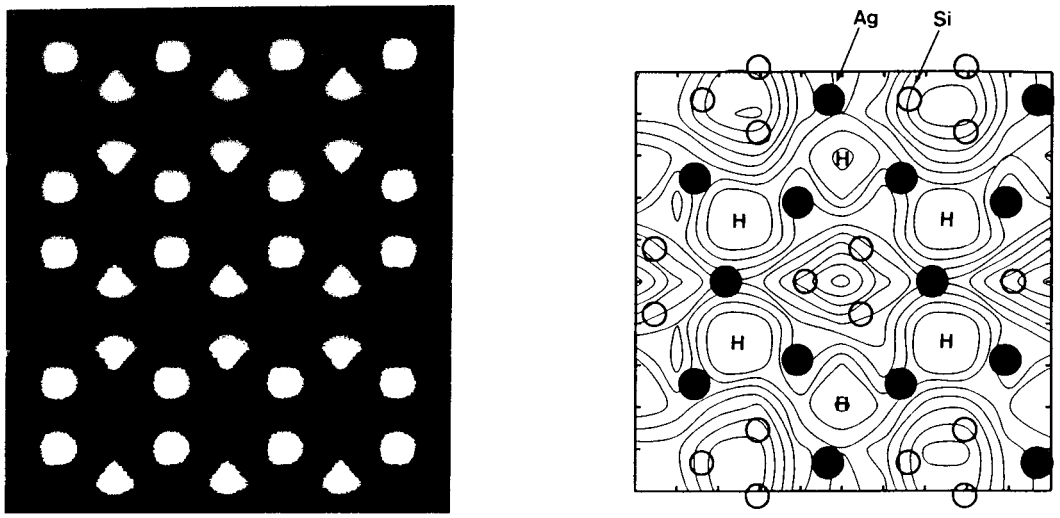

Figure 14. (a) Gray scale image of the calculated tunneling current for ($\sqrt{3}\times\sqrt{3}$)R30° Ag on Si(111) with a logarithmic scale for a bias voltage of −1.0 V applied to the tip. The distance between Ag layer and the outermost W atom of the tip was 3.7 Å. (b) Contour map of the tunneling current in the logarithmic scale under the same conditions. Filled and open circles denote Ag and Si atoms, respectively, and H indicates the maxima of tunnel current. (Reprinted from ref 77. Copyright 1991 American Institute of Physics.)

gives a 0.8 Å bump for an isolated S atom, while in the 2×2 layer the image corrugation is 0.2−0.3 Å. However, the dense layer image is *not* a simple superposition of S atom patterns. Since the tip can be coupled simultaneous to different adatoms, several tunneling paths are possible for the electron and the final image results from the interference between these tunneling paths. In the considered example a constructive interference, when the tip is over the center of a specific triangle of three S atoms, results in a modification of the shape of the adatom image. For a tip ending with a small atom (first class) this effect is negligible, since the tip cannot interact efficiently with several adsorbates. For the metal atom ending tip, the electronic extension is larger and the interference gives the triangle shape. Finally the effect is strong for the large Pt_3 apex, and the current when the tip is over the middle of a triangle of S atoms (i.e. above no adsorbate) is equal to that on the S adsorbate. Similarly a dependence of the image shape on the adsorption site and height of the atom was demonstrated for the dense layer, which vanishes for the isolated case. Therefore the sensitivity of the image to the tip or chemisorption structure seems strongly enhanced for the dense layer, due to the interference effects between adsorbates.

Another example from a very different type of system was given by Tsukada et al. The atomic structure of the ($\sqrt{3}\times\sqrt{3}$)R30° layer of Ag on a Si(111) surface has been a puzzle only recently solved. A model called the honeycomb-chained-trimer (HCT) was proposed,[73] and it is consistent with almost all experimental results. However, the position of the Ag atoms on the surface for this model is not at all in agreement with the position of the bright spots in the STM image.[74−76] Therefore a simple analysis would rule out this model. A calculation[77,78] of the STM image with a +1 V bias on the sample and a W_{10} cluster to model the tip was performed with the HCT model. The bright spots in the image are in excellent agreement with the experimental image and, hence, do not correspond with the positions of Ag atoms. Each bright spot is located at the center of the triangle formed by three Ag atoms and does not correspond to any atom (Figure 14). This is characteristic of the electronic structure and corresponds to the maximum amplitude position of the lowest unoccupied state which consists mainly of Ag 5s and 5p orbitals.

Various concentrations of carbon on Ni(100) have been studied by Hörmandinger et al.[40,79] As explained above, the presence of C leads to a decrease of the density of states at the surface around the Fermi energy and this causes the tip to come closer to the surface in a localized area around the C atom. As the concentration of C grows, this reduction of the density of states becomes more pronounced, so the tip continues to approach the surface. Compared to the bare surface, the average position of the tip moves down by 0.06 Å for the p(2×2) structure (coverage 0.25 monolayer) and 0.19 Å for the c(2×2) structure (0.5 monolayer), in qualitative agreement with the experimental observations.[80] In the case of sulfur on the same surface, the behavior is opposite.[81] The average tip height increases by 0.5 Å between the 0.25 and 0.5 monolayer situations, while the corrugation drops from 0.25 to 0.05 Å. The calculations confirm that the height difference observed between the two images is of electronic origin and is not at all related with a modification of the *z* coordinate of the adsorbate.

Sulfur produces a set of ordered structures on Mo(100) for coverages of 0.5, 0.66, and 0.75 monolayers.[82] For the two lowest coverages, the STM images show a protrusion at each sulfur adsorbate and then directly reflects the structural arrangement of adsorbates.[83] The situation is more complex for the high-coverage c(4×2) structure. Each surface unit cell contains four Mo surface atoms and hence three adsorbed S atoms. However the STM images only show one large protrusion with an important cor-

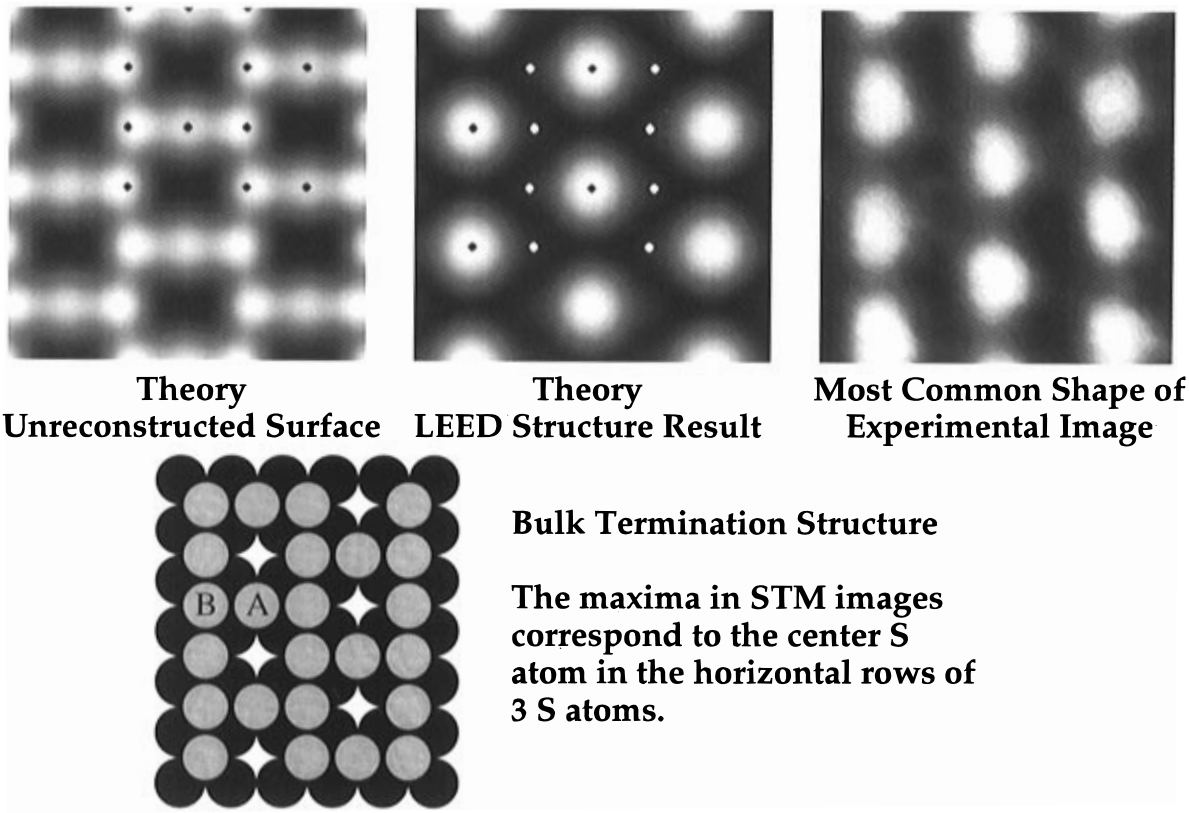

Figure 15. Calculated and experimental topographic images of Mo(100) + c(4×2)-3S, modeled at bottom: (top left) calculated image assuming a bulk-termination "unrelaxed" structure; (top middle) calculated image assuming the relaxed structure found with LEED; both calculated images correspond to a sulfur-terminated tip and to a current of 1nA and a voltage of 50 mV; the black or white dots indicate the positions of the S atoms on the surface; (top right) experimental image. (Reprinted from ref 85. Copyright 1996 Elsevier.)

rugation (0.4−1.2 Å depending on the tip) per unit cell. Therefore the images clearly display the c(4×2) symmetry of the overlayer, but give no direct information on the unit cell content. The situation gets even more intriguing if the LEED structural results is considered:[84] all sulfur atoms occupy similar 4-fold hollow sites, with however two types of S atoms with two (type-A) or three (type-B) S neighbors on the surface (Figure 15). The adsorbate-induced relaxation of the substrate results in a difference in z for the S atoms, the S atoms of type A being 0.2 Å higher. The calculated image with ESQC is very sensitive to the presence of the surface reconstruction.[85] The unrelaxed surface shows a maximum in the image for each S atom. However, as soon as the surface relaxation obtained by LEED is included, the calculated image shows only one maximum on type-A sulfur. On the second type of S atoms, the tip height is ∼1 Å lower, almost the same as on the empty hollow sites, even if their true z coordinates is only 0.2 Å smaller than that of type-A sulfur. This calculated image is in good agreement with the experimental data. The decrease of the tunnel current on type-B S atoms is due to destructive interference effects between tunneling channels involving A and B type adsorbates. This effect amplifies the dependence of the image to atomic positions, the 0.2 Å z difference giving an especially strong destructive effect over B. This destructive interference effect was explained by a different sign on the p_z atomic orbital for type-A and type-B sulfur atoms in the most important electronic states for tunneling.

V. Influence of Imaging Conditions

Most of the images in the previous sections (except on semiconductors) were calculated with a low bias voltage, but still with a relatively large gap resistance (10−100 MΩ), so that the tip is not too close to the adsorbate. Specific effects arise when the bias voltage is increased so that levels further away from the Fermi energy can be probed, or on the contrary when the tunnel gap resistance is decreased and strong tip−surface interactions are switched on. Other aspects on the dependence of the image on the structure of the tip apex will also be discussed in this section.

1. Effect of Bias Voltage

When a low bias voltage is considered, the sample and tip Fermi levels are equalized and only bulk conduction electrons at that energy are involved in the tunnel process. For a perturbative calculation, the LDOS is evaluated at the Fermi energy and for a scattering matrix calculation incoming and outgoing electrons are considered at that same energy. Notice that this does not prevent MO's of the adsorbate at an energy different from the Fermi level to participate via tails of resonances (or in other words, orbital

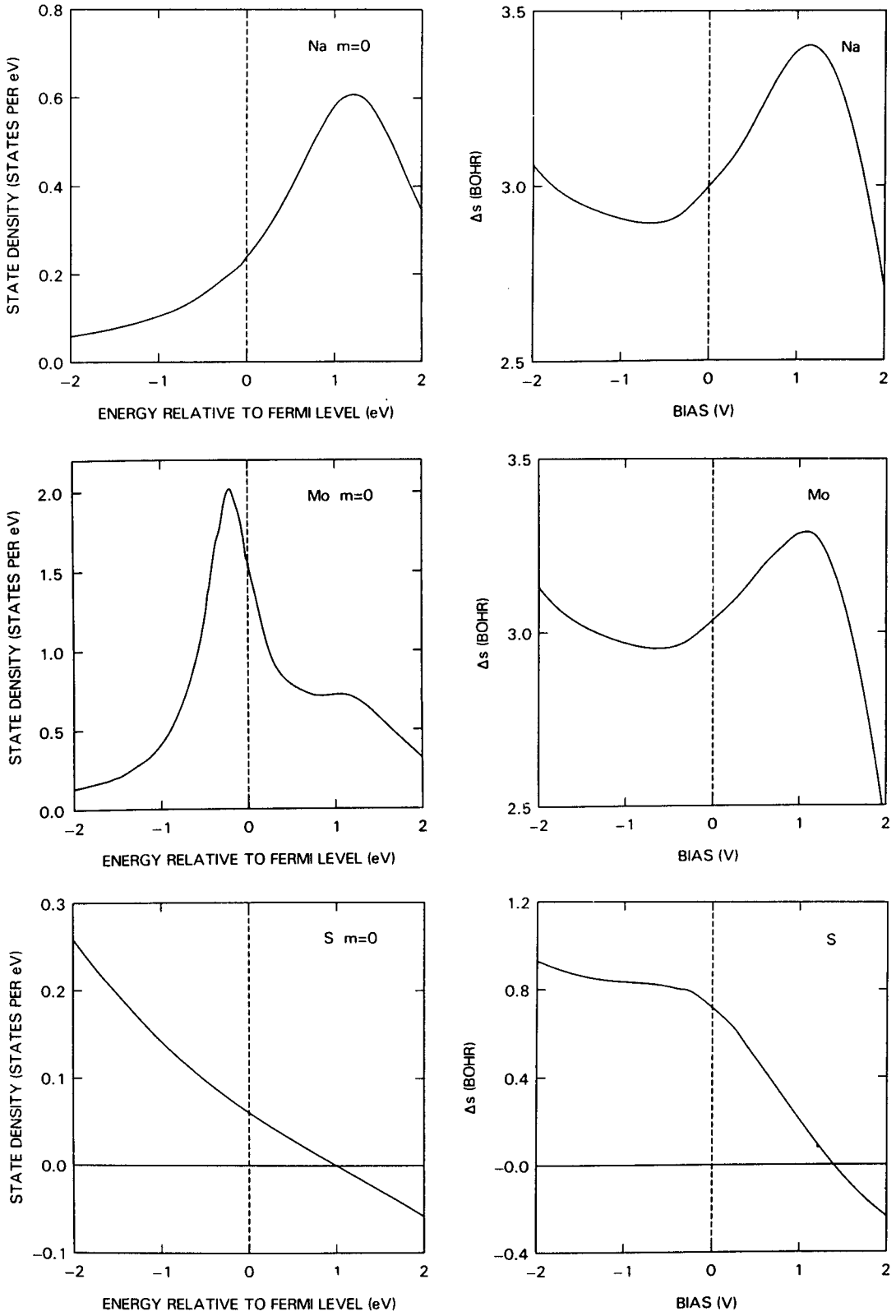

Figure 16. Calculated results for adsorbed Na (top), Mo (middle), and S (bottom) on jellium. Left: Difference in eigenstate density between metal−adatom system and bare metal ($m = 0$ component). Right: tip displacement as a function of applied bias voltage Δs (V). (Reprinted from ref 86. Copyright 1987 American Institute of Physics.)

mixing) in that "tunneling" state. When a finite bias voltage V is applied to the sample, a range of electronic states $[E_f, E_f + |e|V]$ is probed by the tunnel process and the final current is integrated over that interval. If the bias is positive, electrons tunnel into Fermi level and empty states of the sample up to $E_f + |e|V$. On the contrary, they would tunnel from filled states of the sample for a negative bias.

The bias-dependent apparent size of an adatom in a topographic STM image was studied by Lang, for the examples of Na, Mo, and S chemisorbed on jellium (see section III) in order to understand how the image reflects the sample density of states[86,87] (Figure 16). For Na the corrugation increases when probing empty states and this is simply related to the fact that the 3s resonance peak in the DOS is

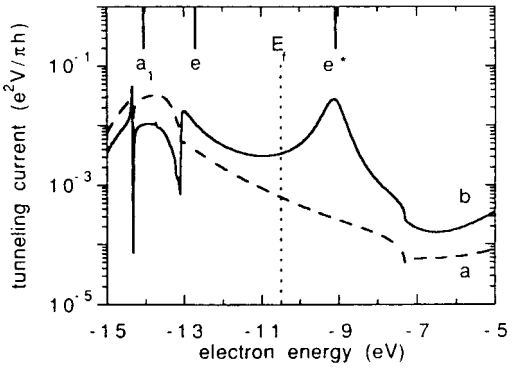

Figure 17. Intensity of the tunneling current for benzene on Rh(111) as a function of the incoming electron for a tip-to-Rh(111) distance of 6.0 Å: (a) intensity in the center of the molecule and (b) on the benzene ring at the lobe maximum. The energy positions of the benzene molecular orbitals and of the Fermi level E_f are indicated. (Reprinted from ref 52. Copyright 1991 Elsevier.)

mostly above the Fermi level. The case of Mo is especially interesting since the DOS shows two features: the large narrow peak below the Fermi level corresponds to 4d orbitals of the atom, while the 5s state appears in a broad and small peak 1 eV above the Fermi level. The tip−sample separation increases for positive bias, reflecting the 5s state resonance but there is no contribution of the 4d states to the topography. These d orbitals are much more contracted as compared to valence s orbitals and hence have a smaller amplitude at the tip. The case of S reflects the tail of the occupied 3p peak. Past 1 eV above the Fermi level, the S atom decreases the state density of the surface. The apparent height is reduced for positive bias, and the contrast is predicted to invert to a depression at ~1.3 eV, reflecting the evolution of the state density.

The adsorption of oxygen on Ag(110) shows an interesting bias voltage effect. Oxygen forms on this surface a (2×1) added-row reconstruction with the formation of −Ag−O−Ag− chains on the surface. The calculated images[88,89] show a clear linelike structure along the added row. For a negative sample bias −1.5 V, the maximum current along the line is positioned over the O atom, while if the sample bias is increased beyond $V = -1.0$ V (up to +0.5 V) the brightest position shifts to the Ag site, and this even though O is farther out of the surface than Ag. This result can be connected with the low bias voltage images that show O adatoms on a flat surface as a depression. States centered on O $2p_z$ orbitals begin 1 eV below the Fermi level, resulting in an increase of the current over O for bias voltages more negative than −1 V. In this case, LDOS images show a behavior markedly different from the calculated current, and this is attributed to an effect of the tip electronic structure, which is properly taken into account in the current calculation.

The influence of bias voltage was also addressed in the case of an adsorbed benzene molecule.[52] For benzene on Rh(111) the tunnel current was calculated as a function of the energy of the incoming electron, which differs from a realistic bias in that only single energies are considered and that the integration in the allowed energy interval $[E_f, E_f + |e|V]$ is not performed (Figure 17). This calculation shows the resonances and their tails crossing the Fermi level. If the tip is positioned over the center of the molecule, only the low-lying a_1 resonance appears by symmetry, while for an off-center position, the resonances corresponding to the e HOMO and e* LUMO states are turned on. Clearly, for the surface Fermi level, the tail from the LUMO orbital is the principal contribution to the tunnel current. Images have been calculated with different electron energies. For energies higher than E_f, the contribution of the LUMO is even increased and this reinforces the 3-fold aspect of the image, the lobes being more clearly separated. By contrast, below the Fermi level, the influence of the LUMO is decreased and the 3-fold shape is weakened, disappearing for an energy 1.5 eV lower than the Fermi level.

Similar variations in the electron energy were used for benzene on graphite.[59] The highest occupied states of the molecule come almost in resonance with the tip Fermi level, 2 eV below E_f, and the image is essentially a charge density map of these orbitals and shows a 6-fold symmetry. The LUMO is almost in resonance, 1.5 eV above E_f, but only a weak 3-fold symmetry is apparent in the image. This difference from Rh(111) can be explained by the smaller interaction between the molecule and the graphite. The same problem of the contrast of benzene on graphite as a function of bias voltage was studied at the same time by Tsukada et al.[90] An approach was developed that combines an analytical theory based on a transfer matrix formalism and first-principles calculations of the electronic states of the adsorbed systems. The assumed adsorption geometry of benzene on graphite is different from that calculated by Fisher et al.[59] The results are however rather similar: the π electron cloud of the molecule is visible at high bias voltage (1 V) while for low bias voltage the substrate is mainly imaged and the benzene molecule is more or less transparent.

Bias-induced changes of the internal contrast of a molecular adsorbate have also been reported in the case of Cu−phthalocyanine.[66] The internal details of the image are completely modified if the electron energy is increased by 1.5 eV, reflecting the participation of different MO's in the contrast. The variation of the transmission coefficient through a C_{60} molecule as a function of the incident electron energy was also calculated with ESQC.[91] The I(V) characteristic was then integrated and found to have a linear behavior for low bias voltages. This is a consequence of the absence of molecular-level resonance in the considered energy window around the Fermi level.

A theory of local tunneling spectroscopy was presented by Baratoff et al.[92,93] They considered tunneling via an isolated molecule, including coupling to a vibrational mode. The conditions under which resonant tunneling with enhanced vibrational excitation can occur have been identified, and the relative features in local I(V) characteristics have been predicted.

2. Influence of the Tip–Surface Separation; Strong Tip–Surface Interaction

In the experiment the tip−surface separation is controlled by the given resistance of the tunnel gap.

It was already noted that, generally speaking, a reduction of the gap resistance, i.e. of the tip−sample distance, results in an increase of the corrugation of the adsorbate since faster changing electronic density regions are probed. More dramatic effects can appear at small tip−sample separation where the Bardeen's perturbative approach breaks down.

Noguera used an approach similar to that of Lang, for a Na atom chemisorbed on a flat metallic "jellium" surface.[94] However, smaller tip-to-surface separations were considered, and the calculations went beyond the transfer Hamiltonian approach, taking into account the tip induced modification of the LDOS (MLDOS) of the surface. The resulting contrast depends on the tip apex structure, a Na tip giving an enhancement of the current, and an electronegative atom tip a reduction, compared to the result of the perturbation approach.

The missing row reconstruction of Cu(110) induced by chemisorption of potassium was studied by Doyen et al.[95] The K atoms sit in the trough of the reconstructed Cu(110) surface, deep inside the first Cu layer. Calculated images at 4.4 Å separation show the top Cu rows as maxima. The K 4s resonance is positioned well below the Fermi level, and the K atom is almost invisible. However at smaller tip−surface separation (2.6 Å), the K atoms appear as protrusions exceeding the Cu maxima, because the tip interacts with the K atoms.[25] Such inversion of the STM image contrast with a modification of the gap resistance has been observed experimentally.

The high coverage p(2×2) structure of Na on Al(111) involves two Na atoms in the unit cell; however, the STM image shows only one bump per unit cell. One Na atom is in a substitutional position within the first Al layer, while the second is on the surface in a fcc hollow position. The tunnel current was calculated[96] at a z of 3.8 Å above the Al surface, and with a bias voltage of −1.2 V i.e. probing occupied sample states. Surprisingly, the highest current is obtained when the tip is over the substitutional Na atom, in contrast with the LDOS which is maximum above the adsorbed Na atom. If the tip−sample separation is increased up to 6.3 Å, the contrast is inverted and the brightest spots are on the Na-fcc atom. The larger distances are more relevant with the STM experiments but contrast inversion was indeed observed at small tip heights.

Tip−surface interactions[97] generally result in forces on the surface and tip apex atoms. These forces are especially exploited in the atomic force microscope, but they can have significant influences in STM. They result in deformations and even atom transfers[98] which can strongly affect the STM contrast. They can be especially important for the imaging of a large and soft adsorbate. Simultaneous calculations of current and tip-induced deformation when imaging an adsorbate are rather rare.

The variation of the tunnel current as a function of the tip apex to surface distance, when the tip is above a C_{60} molecule, was calculated by Joachim et al.[99] in comparison with an experimental measurement on Au(110). The C_{60} deformation was included in the ESQC calculation with a molecular mechanics parametrized approach (MM2 routine[100]) and the

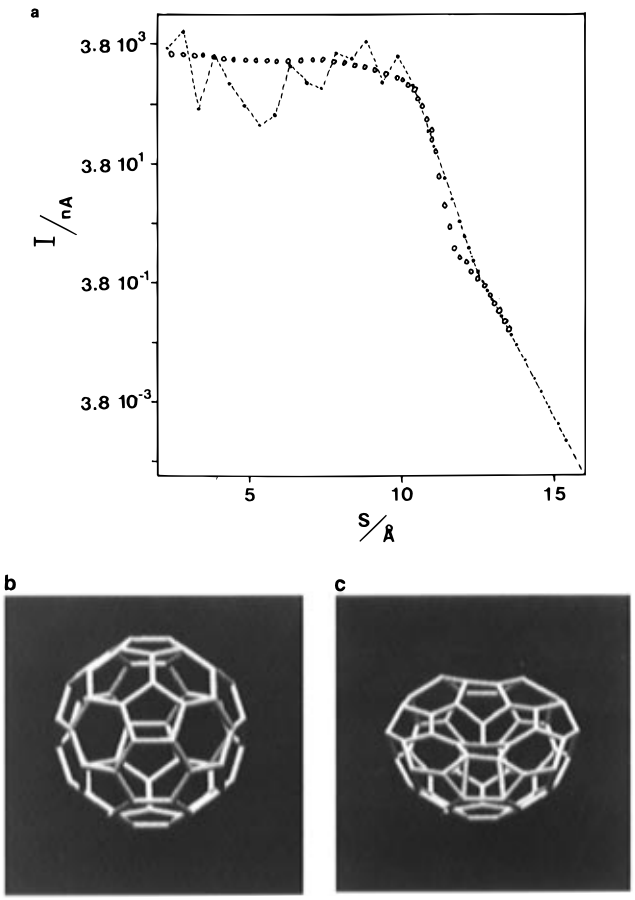

Figure 18. (a) Variation of the tunneling current intensity $I(s)$ through a C_{60} molecule as a function of the tip apex to surface distance s. The open circles indicate the experimental values; the solid line indicates the calculated values with a deformation of C_{60} upon the tip approach. In both cases, a 50 mV bias voltage is chosen. Optimized structure of the C_{60} molecule in the tunneling junction for a tip apex to surface distance of (b) $s = 14$ Å and (c) $s = 7.35$ Å. The W tip apex was considered rigid during the approach. (Reprinted from ref 99. Copyright 1995 American Institute of Physics.)

conformation of the molecule was optimized for each selected tip−surface separation. For a separation lower than 12 Å, the molecule begins to undergo compression and the current increases due to the closure of the C_{60} HOMO−LUMO gap under deformation (Figure 18). At short separations the molecule is almost transparent to the tunneling electrons and the quantum resistance limit is reached. This observation of a pressure dependence in the conductance of an individual C_{60} molecule is a first step toward the understanding of electrical properties of isolated molecules.

Another influence of the tip on the adsorbate is related with the electric field between the tip and substrate. This was studied with self-consistent CNDO calculations and a cluster model by Ramos et al.[101,102] Bardeen's approach was used to calculate the current from the wave function. Isolated carbon monoxide, acrylonitrile (CH_2CHCN), and pyridyl sulfide ($S(C_5H_4N)$) molecules were considered, vertically adsorbed at the C, N, and S atom, respectively. The substrates were Cu(100), Cu(111), and Al(111), and the tip was moving 6 Å above the top of the molecules, with a 2 V bias voltage. Upon interaction

with the electric field, molecules were rotated (up to 15°), distorted, or displaced toward the tip or the sample (up to 0.6 Å). For CO, the effect was a displacement of 0.2 Å toward the tip. In the case of a submonolayer of CO, the STM tip results in a rotation and displacement of the molecules along the surface. The electric field can push the molecule from a 2-fold to a 4-fold site. It is therefore clear that a high bias voltage between tip and surface can have a dramatic effect on the adsorbed molecule. Experimentally, CO on Pt(111) was imaged at low voltage, while a higher bias was used in order to manipulate the molecule.[103]

3. Influence of the Atomic and Electronic Structure of the Tip Apex

In many calculations, the structure of the tip apex is not taken into account. The tip is modeled by a δ function or an s-wave. However, the tip is a very important partner in STM imaging, and the precise structure of the apex can dramatically influence the resulting image, as already discussed above. The main difficulty is that the tip apex structure is not known in the STM experiments, so that various hypotheses have to be considered. The importance of p and d states at the tip apex for the calculated corrugation of bare surfaces has been demonstrated by Chen.[104] The influence of d orbitals at the tip apex on the local electronic structure and current was also underlined by Doyen et al.[105] At short tip−sample distance, a significant part of the tunnel current flows directly via the tip d orbitals.

Sudden changes in the appearance and amplitude of atomic corrugation images of adsorbates are commonly observed in the experiments. These changes are usually attributed to random modification of the tip apex structure, either by atomic diffusion at the tip apex or by atomic transfer from or towards the surface. Variation in the image of a S layer on Pt(111) has been investigated by controlled transfer of atoms between tip and sample and the results were compared with theoretical calculations with ESQC.[106] From the calculations, it was shown that a tip terminated by a Pt atom results in a small current corrugation on the S layer (0.2 nA), while a tip terminated by a S atom would yield a much larger corrugation (more than 1 nA) for a constant height profile with a similar average current value (∼1 nA). The difference can be qualitatively understood by considering the overlap between tip atom orbitals and the adsorbate. The 6s valence orbital of Pt extends farther out in space than the more contracted 3s and 3p of the S atom. The tip terminated by the S atom must be brought by ∼1.5 Å closer to the surface to maintain the same average tunneling current. As a result the current corrugation is larger for the S tip. This calculation clearly and simply relates the electronic size of the tip apex with the image corrugation.

The influence of the tip electronic structure was also particularly studied by Tsukada et al.,[107−110] with various models of W tip apexes, modeled by 10−20 atom clusters. Most of the current is concentrated on a single tip apex atom, if the other atoms at the bottom of the tip are not at the same z level. This situation leads to normal STM images. If there is more than one atom at the same level at the end of the tip, abnormal images are obtained. Applications were given in the case of Ag on Si(111)[107,108] that was already discussed in section IV.

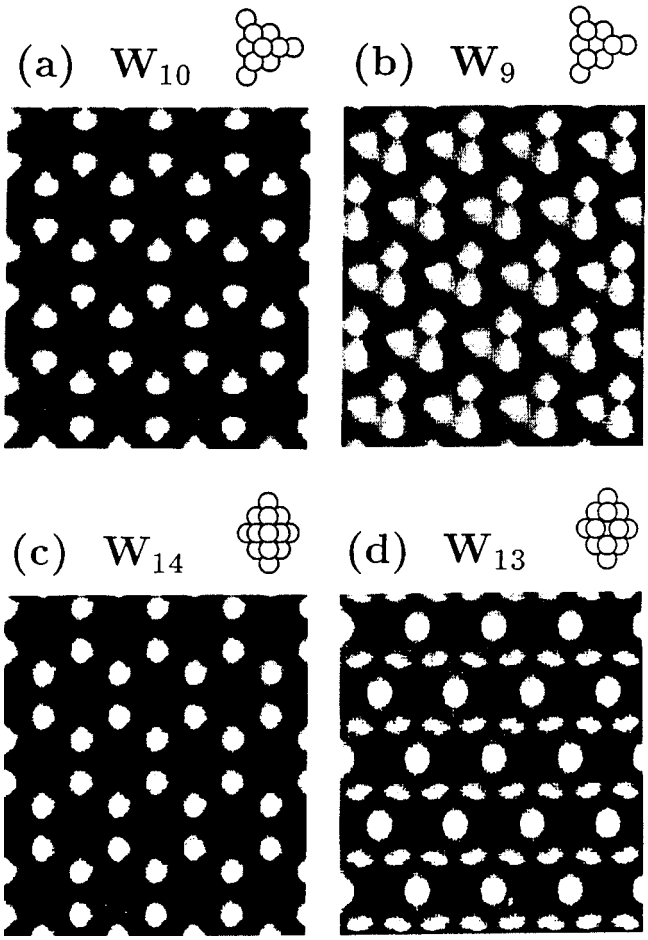

Figure 19. Gray scale images of the tunneling current for ($\sqrt{3}\times\sqrt{3}$)R30° Ag on Si(111) with a logarithmic scale calculated for (a) W_{10}, (b) W_9, (c) W_{14}, and (d) W_{13} tips, with the tip−sample distance of 3.7 Å. Schematic views of the tip models are also shown. (Reprinted from ref 109. Copyright 1994 Slack Inc.)

Four apexes were considered: (a) W_{10} with a [111] orientation; (b) W_9, similar to a but with the apex atom missing; (c) W_{14} with a [110] orientation; and (d) W_{13} similar to c but with the apex atom missing[109] (Figure 19). The apexes a and c, that terminate in a single atom, give the same image with the honeycomb arrangement of bright spots. Tips b and d terminate in three or four atoms at the same z, and the images show quite different image patterns, and differ from each other. Notice that the symmetry of the tip can affect the symmetry of the image, as is the case for the d tip.[110] The influence of a tilt of b and d apexes was examined. The abnormal images recover a normal shape with only a tilt of ∼20°, since this allows the tunnel current to be concentrated on a single W atom at the apex. When the current flows through more than one atom at the tip apex, interference effects appear but the qualitative features of the image can be reproduced by a simple superposition of tunnel current. However, interference effects cannot be neglected for some specific orientations of the tip.

VI. Conclusion

The interpretation of images of adsorbates obtained with the scanning tunneling microscope is not simple and straightforward. It seems important to go beyond visual inspection and to develop a detailed analysis with the help of theoretical simulations and other experimental techniques. In many cases, and especially for molecules, bumps in the images are not located at the position of atoms and experimental conditions can influence the contrast. Several theoretical approaches have been developed with different levels of approximations for the wave function and tunnel current calculations. Although none of these approaches can claim a fully realistic or quantitative simulation of the STM images, several insights and concepts have been proposed that can be an important help to better understand the images and to extract more information from them.

For the imaging of adsorbates with the STM, it is not correct to say that the microscope images the adsorbate, or that it images the adsorbate perturbed by its interaction with the substrate. The microscope in fact probes the adsorbate *and* the substrate, both perturbed by their mutual interaction. Depending on the system, the direct contribution of the electronic states of the adsorbate is more or less strong, but in many cases it is not possible to neglect the contribution of the substrate itself, these contributions interfering to give the final image. In the case of metal surfaces, where adsorbate interaction is usually strong, the general case is that the contribution of the substrate to the tunnel current is decreased in the region of the adsorbate, i.e. creates a depression. This is not the case for graphite where the interaction is weaker. The direct contribution of the adsorbate to the current is a bump. The lowering of molecular symmetry at the surface site allows orbital mixing and can create an internal structure in the image which reflects the symmetry of the binding site. As a consequence, the STM image is dependent on the binding site of the molecule.

In the general case, the adsorbate has no MO at the substrate Fermi energy. Nonresonant tuneling occurs and the contribution of the adsorbate to the current comes from tails of MO resonances crossing the Fermi level. These tails are usually rather small at the Fermi level, compared to resonant tuneling, which explains why contributions from the substrate itself cannot be neglected, despite the rather important difference in height. Together with the more contracted nature of adsorbate atomic orbitals, compared for example with a valence s orbital of a metal surface atom, this explains the usually small z amplitude of topographic images of adsorbates, compared to the real z coordinate of the adsorbate. A larger bias voltage in the experiment (typically ± 1 V) increases the contribution of occupied or vacant MO's depending on the sign. In most cases, it is not correct to say that the image shows one MO of the adsorbate, LUMO or HOMO. A larger number of MO's above and below the Fermi level need to be included in order to accurately describe the tunnel current. The contribution of a given MO can be understood in terms of its energetic distance with the Fermi level, and also of the strength of its interactions with surface and tip. Moreover these contributions from MO's can strongly interfere with each other and this can have a large influence on the final contrast.

Due to the delocalized nature of MO's, the image of a molecular adsorbate does not show the atoms but the pattern is characteristic of the molecule, and it allows a shape recognition of the molecule, distinguishing between isomers.

A specific aspect arises in the case of dense layers of adsorbates, as shown in the case of atoms. In this case, if the electronic radius of the tip is large enough, it can interact with several adsorbates at the same time and electronic interferences between these different tunneling channels can strongly affect the image and give a strong dependence on the tip apex structure. The current maxima can then be positioned in between atoms, or two symmetry-inequivalent adsorbates on the surface can show markedly different contrast. These electronic effects tend to create STM topographic images that can be strongly different from the geometric structure of the substrate.

Experimental conditions can also have a large influence on the contrast. A change of bias modifies the energy of the electrons and probes differents parts of the electronic structure, opening the way to spectroscopic measurements. A small tunnel conductance gives a short tip−surface separation. Perturbative approaches are not applicable any more and the strong tip−surface interaction can affect the contrast and even invert the image in some cases. Forces are present between tip and surface: they can displace the molecules, or distort and compress them. Such a compression can give a strong amplification of the tunnel current, by a perturbation of the electronic structure of the molecule. Finally, the tip shape can be an important and often poorly characterized element. However, the dependence of the image on the tip structure is not too dramatic, especially for well-separated adsorbates, because as soon as one atom is significantly lower than the others at the tip apex, most of the current flows through that individual atom.

Many pitfalls and difficulties were underlined in this review. However STM is a wonderful tool that provides local "atomic" resolution information of an adsorbate on a surface. It is hoped that the insights and warnings presented here will allow a richer and more precise analysis and understanding of a constantly growing number of high quality STM images.

VII. References

(1) Hoffmann, R. *Rev. Mod. Phys.* **1988**, *60*, 601.
(2) Kohn, W.; Sham, L. J. *Phys. Rev. A* **1965**, *140*, 1133.
(3) Bardeen, J. *Phys. Rev. Lett.* **1961**, *6*, 57.
(4) Tersoff, J.; Hamann, D. R. *Phys. Rev. Lett.* **1983**, *50*, 1998.
(5) Tersoff, J.; Hamann, D. R. *Phys. Rev. B* **1985**, *31*, 805.
(6) Tersoff, J. *Phys. Rev. B* **1989**, *40*, 11990.
(7) Noguera, C. *J. Phys. (Paris)* **1989**, *50*, 2587.
(8) Chen, C. J. *Introduction to Scanning Tunneling Microscopy*; Oxford University Press: New York, 1993.
(9) Chen, C. J. In *Scanning Tunneling Microscopy III*; Wiesendanger, R., Güntherodt, H. J., Eds.; Springer Series in Surface Science 29; Springer-Verlag: Berlin, 1993; p 141.
(10) Chen, C. J. *J. Vac. Sci. Technol. A* **1991**, *9*, 44.
(11) Tsukada, M.; Kobayashi, K.; Isshiki, N.; Kageshima, H.; Uchiyama, T.; Watanabe, S.; Schimizu, T. *Surf. Sci. Rep.* **1991**, *13*, 265.

(12) Tsukada, M.; Kageshima, H.; Isshiki, N.; Kobayashi, K. *Surf. Sci.* **1992**, *266*, 253.
(13) Tsukada, M.; Kobayashi, K.; Isshiky, N.; Watanabe, S. In *Scanning Tunneling Microscopy III*; Wiesendanger, R., Güntherodt, H. J., Eds.; Springer Series in Surface Science 29; Springer-Verlag: Berlin, 1993; p 77.
(14) Sacks, W.; Noguera, C. *J. Vac. Sci. Technol. B* **1991**, *9*, 488.
(15) Sacks, W.; Noguera, C. *Phys. Rev. B* **1991**, *43*, 11612.
(16) Sacks, W.; Noguera, C. *Ultramicroscopy* **1992**, *42*−*44*, 140.
(17) Tekman, E.; Ciraci, S. *Phys. Rev. B* **1989**, *40*, 10286.
(18) Ciraci, S.; Baratoff, A.; Batra, I. P. *Phys. Rev. B* **1990**, *42*, 7618.
(19) Becker, R. S.; Golovchenko, J. A.; McRae, E. G.; Swartzentruber, B. S. *Phys. Rev. Lett.* **1985**, *55*, 2028.
(20) Kubby, J. A.; Wang, Y. R.; Greene, W. J. *Phys. Rev. Lett.* **1991**, *65*, 2165.
(21) Pendry, J. B.; Prêtre, A. B.; Krutzen, B. C. H. *J. Phys. C* **1991**, *3*, 4313.
(22) Lucas, A. A.; Vigneron, J.-P.; Lambin, Ph.; Laloyaux, Th.; Dericke, I. *Surf. Sci.* **1992**, *269/270*, 74.
(23) Vigneron, J.-P.; Dericke, I.; Lambin, Ph.; Laloyaux, Th.; Lucas, A. A.; Libioulle, L.; Ronda, A. *Ultramicroscopy* **1992**, *42*−*44*, 250.
(24) Doyen, G.; Koetter, E.; Vigneron, J. P.; Scheffler, M. *Appl. Phys. A* **1990**, *51*, 281.
(25) Doyen, G. In *Scanning Tunneling Microscopy III*; Wiesendanger, R., Güntherodt, H. J., Eds.; Springer Series in Surface Science 29; Springer-Verlag: Berlin, 1993; p 23.
(26) Sautet, P.; Joachim, C. *Phys. Rev. B* **1988**, *38*, 12238.
(27) Kenkre, V. M.; Biscarini, F.; Bustamante, C. *Ultramicroscopy* **1992**, *42*−*44*, 122.
(28) Kenkre, V. M.; Biscarini, F.; Bustamante, C. *Phys. Rev. B* **1995**, *51*, 11074.
(29) Lang, N. D. *Phys. Rev. Lett.* **1985**, *55*, 230.
(30) Lang, N. D. In *Scanning Tunneling Microscopy III*; Wiesendanger, R., Güntherodt, H. J., Eds.; Springer Series in Surface Science 29; Springer-Verlag: Berlin, 1993; p 7.
(31) Lang, N. D. *Phys. Rev. Lett.* **1986**, *56*, 1164.
(32) Lang, N. D. *Comments Condens. Matter Phys.* **1989**, *14*, 253.
(33) Klink, C.; Olesen, L.; Besenbacher, F.; Stensgaard, I.; Laegsgaard, E.; Lang, N.D. *Phys. Rev. Lett.* **1993**, *71*, 4350.
(34) Eigler, D. M.; Weiss, P. S.; Schweizer, E. K.; Lang, N. D. *Phys. Rev. Lett.* **1991**, *66*, 1189.
(35) Bouju, X.; Joachim, C.; Girard, C.; Sautet, P. *Phys. Rev. B* **1993**, *47*, 7454.
(36) Mahanty, J.; Tsukada, M. *Surf. Sci.* **1991**, *258*, L679.
(37) Doyen, G.; Drakova, D.; Kopatzki, E.; Behm, R. J. *J. Vac. Sci. Technol. A* **1988**, *6*, 327.
(38) Lang, N. D. *Phys. Rev. B* **1988**, *37*, 10395.
(39) Jacobsen, J.; Hammer, B.; Jacobsen, K. W.; Norskov, J. K. *Phys. Rev. B* **1995**, *52*, 14954.
(40) Hörmandinger, G.; Pendry, J. B. *Surf. Sci.* **1994**, *303*, 197.
(41) Biscarini, F.; Bustamante, C.; Kenkre, V. M. *Phys. Rev. B* **1995**, *51*, 11089.
(42) Sautet, P. *Surf. Sci.* **1997**, *374*, 406.
(43) Clementi, E.; Roetti, C. *At. Data Nucl. Data Tables* **1974**, *14*, 177. McLean, A. D.; McLean, R. S. *At. Data Nucl. Data Tables* **1981**, *26*, 197.
(44) Stroscio, J. A.; Eigler, D. M. *Science* **1991**, *254*, 1319.
(45) Zeppenfeld, P.; Lutz, C. P.; Eigler, D. M. *Ultramicroscopy* **1992**, *42*−*44*, 128.
(46) Bocquet, M.-L.; Sautet, P. *Surf. Sci.* **1996**, *360*, 128.
(47) Lambin, G.; Delvaux, M. H.; Calderone, A.; Lazzaroni, R.; Brédas, J. L.; Clarke, T.C.; Rabe, J. P. *Mol. Cryst. Liq. Cryst.* **1993**, *235*, 75.
(48) Brédas, J. L.; Street, G. B. *J. Am. Chem. Soc.***1988**, *110*, 7001.
(49) Brédas, J. L.; Street, G. B. *J. Chem. Phys.* **1989**, *90*, 7291.
(50) Chiang, S. In *Scanning Tunneling Microscopy I*; Güntherodt, H. J., Wiesendanger, R., Eds.; Springer-Verlag: Berlin, 1992; p 181.
(51) Ohtani, H.; Wilson, R. J.; Chiang, S.; Mate, C. M. *Phys. Rev. Lett.* **1988**, *60*, 2398.
(52) Sautet, P.; Joachim, C. *Chem. Phys. Lett.* **1991**, *185*, 23.
(53) Lin, R. F.; Blackmann, G. S.; Van Hove, M. A.; Somorjai, G. A. *Acta Crystallogr. B* **1987**, *43*, 368.
(54) Sautet, P.; Dunphy, J.; Salmeron, M. In *Elementary Reaction Steps in Heterogeneous Catalysis*; Joyner, R. W., Van Santen, R. A., Eds.; NATO ASI C 398; Kluwer Academic Publishers: Dordrecht, 1993; p 305.
(55) Sautet, P.; Joachim, C.; Bocquet, M.-L.; Salmeron, M. *Ann. Chim. Fr.* **1992**, *17*, 217.
(56) Hallmark, V. M.; Chiang, S. *Surf. Sci.* **1995**, *329*, 255.
(57) Weiss, P. S.; Eigler, D. M. *Phys. Rev. Lett.* **1993**, *71*, 3139.
(58) Weiss, P. S. *Trends Anal. Chem.* **1994**, *13*, 61.
(59) Fisher, A. J.; Blöchl, P. E. *Phys. Rev. Lett.* **1993**, *70*, 3263.
(60) Sautet, P.; Bocquet, M. L. *Surf. Sci.* **1994**, *304*, L445.
(61) Sautet, P.; Bocquet, M. L. *Isr. J. Chem.* **1996**, *36*, 63.
(62) Sautet, P.; Bocquet, M. L. *Phys. Rev. B* **1996**, *53*, 4910.
(63) Sautet, P.; Joachim, C. *Ultramicroscopy* **1992**, *42*−*44*, 115.
(64) Hallmark, V. M.; Chiang, S.; Meinhardt, K.-P.; Hafner, K. *Phys. Rev. Lett.* **1993**, *70*, 3740.
(65) Ramos, M. M. D. *J. Phys. C.* **1993**, *5*, 2843.
(66) Sautet, P.; Joachim, C. *Surf. Sci.* **1992**, *271*, 387.
(67) Chavy, C.; Joachim, C.; Altibelli, A. *Chem. Phys. Lett.* **1993**, *214*, 569.
(68) Hui Ou-Yang, Marcus, R. A.; Källebring, B. *J. Chem. Phys.* **1994**, *100*, 7814.
(69) Hwang, R. Q.; Zeglinsky, D. M.; Ogletree, D. F.; Lopez Vazquez-de-Parga, A.; Somorjai, G. A.; Salmeron, M. *Phys. Rev. B* **1991**, *44*, 1914.
(70) Dunphy, J.; Ogletree, D. F.; Salmeron, M.; Sautet, P.; Bocquet, M.-L. *Ultramicroscopy* **1992**, *42*−*44*, 490.
(71) Sautet, P.; Dunphy, J.; Ogletree, D. F.; Salmeron, M. *Surf. Sci.* **1993**, *295*, 347.
(72) Sautet, P.; Dunphy, J. C.; Ogletree, D. F.; Joachim, C.; Salmeron, M. *Surf. Sci.* **1994**, *315*, 127.
(73) Katayama, M.; Williams, R. S.; Kato, M.; Nomura, E.; Aono, M. *Phys. Rev. Lett.* **1991**, *66*, 2762.
(74) Wilson, R. J.; Chiang, S. *Phys. Rev. Lett.* **1987**, *58*, 369.
(75) Van Loenen, E. J.; Demuth, J. E.; Tromp, R. M.; Hamers, R. J. *Phys. Rev. Lett.* **1987**, *58*, 373.
(76) Wilson, R. J.; Chiang, S. *Phys. Rev. Lett.* **1987**, *59*, 2329.
(77) Watanabe, S.; Aono, M.; Tsukada, M. *Phys. Rev. B* **1991**, *44*, 8330.
(78) Watanabe, S.; Aono, M.; Tsukada, M. *Surf. Sci.* **1993**, *287*−*288*, 1036.
(79) Hörmandinger, G.; Pendry, J. B.; Leibsle, F. M.; Murray, P. W.; Joyner, R. W.; Thornton, G. *Phys. Rev. B.* **1993**, *48*, 8356.
(80) Schmid, M.; Biedermann, A.; Varga, P. *Surf. Sci.* **1993**, *294*, L952.
(81) Partridge, A.; Tatlock, G.; Leibsle, F. M.; Flipse, C. F. J.; Hörmandinger, G.; Pendry, J. B. *Phys. Rev. B* **1993**, *48*, 8267.
(82) Dunphy, J. C.; Sautet, P.; Ogletree, D. F.; Salmeron, M. B. *J. Vac. Sci. Technol. A* **1993**, *11*, 1975.
(83) Dunphy, J. C.; Sautet, P.; Ogletree, D. F.; Salmeron, M. *Phys. Rev. B* **1995**, *52*, 11446.
(84) Jentz, D.; Rizzi, S.; Barbieri, A.; Kelly, D.; Van Hove, M. A.; Somorjai, G. A. *Surf. Sci.* **1995**, *329*, 14.
(85) Sautet, P.; Dunphy, J. C.; Salmeron, M. B. *Surf. Sci.* **1996**, *364*, 345.
(86) Lang, N. D. *Phys. Rev. Lett.* **1987**, *58*, 45.
(87) Lang, N. D. *Phys. Rev. B* **1986**, *34*, 5947.
(88) Schimizu, T.; Tsukada, M. *Solid State Commun.* **1993**, *87*, 193.
(89) Schimizu, T.; Tsukada, M. *J. Vac. Sci. Technol B* **1994**, *12*, 2200.
(90) Tsukada, M.; Kobayashi, K.; Isshiki, N. *Appl. Surf. Sci.* **1993**, *67*, 235.
(91) Joachim, C.; Gimzewski, J. K. *Europhys. Lett.* **1995**, *30*, 409.
(92) Baratoff, A.; Persson, B. N. J. *J. Vac. Sci. Technol. A* **1988**, *6*, 331.
(93) Persson, B. N. J.; Baratoff, A. *Phys. Rev. Lett.* **1987**, *59*, 339.
(94) Noguera, C. In *Scanning Tunneling Microscopy III*; Wiesendanger, R., Güntherodt, H. J., Eds.; Springer-Verlag: Berlin, 1993; p 51.
(95) Doyen, G.; Drakova, D.; Barth, J. V.; Schuster, R.; Gritsch, T.; Behm, R. J.; Ertl, G. *Phys. Rev. B* **1993**, *48*, 1738.
(96) Drakova, D.; Doyen, G.; Maca, F. *Surf. Sci.* **1996**, *352*−*354*, 704.
(97) Ciraci, S. In *Scanning Tunneling Microscopy III*; Wiesendanger, R., Güntherodt, H. J., Eds.; Springer Series in Surface Science 29; Springer-Verlag: Berlin, 1993; p 179.
(98) Landman, U.; Luedtke, W. D. In *Scanning Tunneling Microscopy III*; Wiesendanger, R., Güntherodt, H. J., Eds.; Springer Series in Surface Science 29; Springer-Verlag: Berlin, 1993; p 141.
(99) Joachim, C.; Gimzewski, J. K.; Schlittler, R. R.; Chavy, C. *Phys. Rev. Lett.* **1995**, *74*, 2102.
(100) Allinger, N. L.; Kok, R. A.; Iman, M. R. *J. Comput. Chem.* **1988**, *9*, 591.
(101) Ramos, M. M. D.; Stoneham, A. M.; Sutton, A. P.; Pethica, J. B. *J. Phys.: Condens. Matter* **1990**, *2*, 5913.
(102) Ramos, M. M. D.; Sutton, A. P.; Stoneham, A. M. *J. Phys.: Condens. Matter.* **1991**, *3*, S127.
(103) Zeppenfeld, P. *New Sci.* **1991**, *20*, 1757.
(104) Chen, C. J. *Phys. Rev. Lett.* **1990**, *65*, 448.
(105) Doyen, G.; Koetter, E.; Barth, J.; Drakova, D. In *Scanning Tunneling Microscopy and related methods*; Behm, R. J., et al., Eds.; Kluwer: Dordrecht, 1990; p 97.
(106) McIntyre, B. J.; Sautet, P.; Dunphy, J. C.; Salmeron, M.; Somorjai, G. A. *J. Vac. Sci. Technol B* **1994**, *12*, 1751.
(107) Tsukada, M.; Schimizu, T.; Watanabe, S.; Isshiki, N.; Kobayashi, K. *Jpn. J. Appl. Phys.* **1993**, *32*, 1352.
(108) Tsukada, M.; Kobayashi, K.; Isshiki, N.; Kageshima, H.; Uchiyama, T.; Watanabe, S.; Schimizu, T. *Surf. Sci.* **1993**, *287*−*288*, 1004.
(109) Watanabe, S.; Aono, M.; Tsukada, M. *J. Vac. Sci. Technol B* **1994**, *12*, 2167.
(110) Watanabe, S.; Aono, M.; Tsukada, M. *Appl. Surf. Sci.* **1992**, *60*−*61*, 437.

CR9600823